NASA CR-2560

NASA CONTRACTOR REPORT

NASA CR-2

EXPERIMENTAL STUDIES OF FLOW SEPARATION AND STALLING ON A TWO-DIMENSIONAL AIRFOIL AT LOW SPEEDS

H. C. Seetharam and W. H. Wentz, Jr.

Prepared by
WICHITA STATE UNIVERSITY
Wichita, Kans.
for Langley Research Center

NATIONAL AERONAUTICS AND SPACE ADMINISTRATION • WASHINGTON, D. C. • JULY 1975

1. Report No. NASA CR-2560	2. Government Accession No.	3. Recipient's Catalog No.
4. Title and Subtitle EXPERIMENTAL STUDIES OF FLOW SEPARATION AND STALLING ON A TWO-DIMINSIONAL AIRFOIL AT LOW SPEEDS		5. Report Date JULY 1975
		6. Performing Organization Code
7. Author(s) H. C. Seetharam and W. H. Wentz, Jr.		8. Performing Organization Report No.
		10. Work Unit No.
9. Performing Organization Name and Address Wichita State University Wichita, KS		
		11. Contract or Grant No. NGR 17-003-021
		13. Type of Report and Period Covered Contractor Report
12. Sponsoring Agency Name and Address National Aeronautics & Space Administration Washington, DC 20546		
		14. Sponsoring Agency Code

15. Supplementary Notes

16. Abstract

Detailed measurements of flow fields associated with low speed turbulent boundary layers have been made for the 17% thick GA(W)-1 airfoil section at nominal angles of attach of $10°$, $14°$, and $18°$, Reynolds number 2.2×10^6, and Mach number 0.13. The data include extensive pressure and velocity surveys of the pre- and post-separated regions on the airfoil and the associated wake. The boundary layer characteristics including regions of separation on the airfoil are also presented.

17. Key Words (Suggested by Author(s)) Flow separation Airfoil stall GA(W)-1 airfoil Low speed boundary layers	18. Distribution Statement Unclassified - Unlimited Subject Category 02		
19. Security Classif. (of this report) Unclassified	20. Security Classif. (of this page) Unclassified	21. No. of Pages 64	22. Price* $4.25

SUMMARY

Detailed measurements of flow fields associated with low speed turbulent boundary layers have been made for the 17% thick GA(W)-1 airfoil section at nominal angles of attack of 10°, 14°, and 18°, Reynolds number 2.2 x 10^6, and Mach number 0.13. The data includes extensive pressure and velocity surveys of the pre- and post-separated regions on the airfoil and the associated wake. The boundary layer characteristics including regions of separation on the airfoil are also presented.

The results indicate steep gradients of displacement thickness, momentum thickness, shape factor and the separation streamline from the point of separation to the trailing edge of the airfoil. The present tests reveal that the region of flow reversal terminates within a surprisingly short distance of less than 20% chord downstream from the trailing edge for the test range of angle of attack.

INTRODUCTION

The complex phenomena of the interaction between potential and viscous flow fields associated with airfoils has been mathematically modeled by various research groups (Refs. 1, 2, 3). The results of these computer programs show that with the exception of drag estimation the modeling is highly accurate for prediction of the performance of airfoils up to the onset of flow separation. References 1 and 2, however, cannot predict the post-separated boundary layer behavior.

Several methods have been proposed to handle the post-separated boundary layer behavior (Refs. 3, 4, 5). References 3 and 4 base their analysis on the observed constant pressure distribution in the separated regions, whereas Reference 5 approaches the problem using an extension of boundary layer

theory to include regions of separation. These models work reasonably well when the depths of separated regions are small, but fail with large regions of separated flow.

The present experimental investigation is carried out in order to furnish a set of detailed boundary layer characteristics under the influence of extensive separated flow conditions on a low speed airfoil. This data is intended to help the development of better mathematical models for separated flows.

SYMBOLS

To the maximum extent possible, physical measurements are presented in non-dimensional form. Where dimensional quantities are required, they are given in both International (SI) Units and U. S. Customary Units. Measurements were made in U. S. Customary Units. Conversion factors between SI Units and U.S. Customary Units are given in Reference 6. The symbols used in the present report are defined as follows:

c	Wing chord
c_{p_S}	Static pressure coefficient, $\dfrac{p_S - p_\infty}{q_\infty}$
c_{p_T}	Total pressure coefficient, $\dfrac{p_T - p_\infty}{q_\infty}$
H	Shape factor (δ^* / δ^{**})
p_S	Local static pressure
p_T	Local total pressure
p_∞	Free stream static pressure
q_∞	Free stream dynamic pressure
RN	Reynolds number based upon wing chord
U	Velocity at the edge of the boundary layer, non-dimensionalized with respect to free stream velocity.

2

u	Local velocity non-dimensionalized with respect to free stream velocity, $\sqrt{\dfrac{P_T - P_s}{q_\infty}}$
u_x	Component of local velocity in the free stream direction, non-dimensionalized with respect to free stream velocity.
x	Streamwise coordinate
y	Spanwise coordinate
z	Vertical coordinate
α	Angle of attack, degrees
δ	Boundary layer thickness
δ^*	Boundary layer displacement thickness, $\int_{o}^{\delta}(1 - \dfrac{u}{U})dz$
δ^{**}	Boundary layer momentum thickness, $\int_{o}^{\delta}\dfrac{u}{U}(1 - \dfrac{u}{U})dz$

APPARATUS AND PROCEDURE

TEST

The experimental investigations were carried out in the WSU 213 cm x 305 cm (7' x 10') low speed wind tunnel fitted with a 213 cm x 91.4 cm (7' x 3') two-dimensional insert employing a 17% thick GA(W)-1 airfoil section having 61.0 cm (24") chord and a 91.4 (36") span. Details of the construction of the model, supporting disks and the surface pressure taps are given in Reference 7. All tests were conducted with flap nested and at angles of attack of 10.3°, 14.4°, and 18.4°, which represent pre-stall, near-stall, and post-stall conditions respectively. Reynolds number of the test was 2.2×10^6 based on the airfoil chord and Mach number was 0.13. In order to ensure transition, 2.5 mm (0.1") wide strips of #80 carborundum grit were employed at 5% chord on both upper and lower surfaces (Ref. 8). In this test series details of the flow field were investigated only on the upper surface of the model. At each angle of attack pressure measurements were made at ten chordwise stations in order to study the behavior of the boundary layer upstream, downstream and near the separation point on

3

the airfoil. Pressure measurements for determining velocities were also made at four stations downstream of the trailing edge of the airfoil in order to obtain a complete picture of the development of the wake with flow reversal.

INSTRUMENTATION

Velocities were obtained by employing three types of probes (Fig. 1). The five tube pressure sensing pitch-yaw probe of 3.2 mm (.125") diameter was used to obtain velocity profiles for heights more than 2.5 mm (.10") above the local surface of the airfoil. For heights of 5.4 mm (.213") and less, velocities were obtained by employing either a flat tube probe or a cylindrical tube probe for total pressure measurements and model surface orifices for local static pressure measurements. At certain downstream chordwise stations with shallow regions of separation, difficulty was experienced while scanning the reversed flows with the flat tube probe due to the interference of the probe stem on the upstream flow. Hence a cylindrical tube of a 0.46 mm diameter, sealed at one end, with a .3 mm dia. hole drilled at a distance of .38 mm from·the tip was used to scan the stations at and downstream of the separation point. The probes were fixed to a mechanism which has provisions for remote traversing in the vertical axis and remote rotation of ±180° about the probe axis. The traversing gear was mounted to an aluminum channel fixed to the tunnel ceiling. Thus the probes could be locked in position at any chordwise station between the leading edge and 200% chord. The maximum vertical range available for probe travel varied from about 11.4 cm (4.5") to 39.4 cm (12") depending on the chordwise probe location. Unbonded strain gage pressure transducers with a range of ±17.2 Kilo-newtons/m^2 (±2.5 psi) were utilized for all pressure measurements.

METHODS

Surface pressures were obtained through a system of pressure switches and transducers with digital data recorded on punch cards.

Tuft surveys and oil flow methods were employed for observation of the surface flow patterns. In order to obtain qualitative information regarding the depth and the longitudinal growth of the reversed flow regions, tufted spokes of about 1.5 mm (.0625") diameter and 15.2 cm (6") long were fixed to the surface at every 10% chordwise station on the airfoil. These spokes were offset by about 3.8 cm (1.5") in the spanwise direction in order to avoid interference of the tufts. The flow pattern downstream of the trailing edge and the wake was observed by employing tuft spokes at 100% chord, 110% chord, and 120% chord stations. These spokes were located at the midspan and were supported by horizontal rods fixed to the endplate disks to which the model was fitted.

Flow field velocity data was acquired by initially tilting the five-tube probe to align with the local airfoil slope. The probe was then yawed into the plane of the local flow and all five pressures were recorded on punched cards along with probe position. Velocities close to the wall were obtained by aligning either the flat tube probe or the cylindrical tube probe with the direction of the local surface. While scanning the wake regions, the five tube probe was initially aligned horizontally (the free stream direction) and yawed as required into the local flow.

DATA REDUCTION

Surface pressures, local velocities, and flow inclinations were calculated by the computer routine developed for the IBM 1130 computer at WSU. The local velocity is expressed in a non-dimensional form as the ratio of local to free stream velocity. Experimental velocity profiles were plotted by employing a computer plotting routine written for the IBM 1130.

The five tube probe was calibrated through a pitch angle range of ±45°, under dynamic pressures of 479 and 2874 newtons per meter^2 (10 and 60 psf) with probe extensions of 25.4 cm and 40.6 cm (10" and 16") in order to explore the effects of dynamic

pressure and the support interference. No noticeable deviations were observed. Calibration curves were extrapolated up to a maximum pitch angle of ±50° to evaluate velocities. Based on the calibration data, polynomial curve fits were employed for subsequent use in the data reduction program. The inputs for the data reduction program are the five pressures, which are fed into the calibration equations to compute the pitch angle, static pressure, total pressure and velocity. For probe measurements near the airfoil surface (within 5 probes diameters), the image effect of the probe due to the proximity of the wall influences probe readings. Corrections for these effects are included in the computing routine. A more detailed account of the calibration procedure and the results is given in Reference 9.

The flow in the turbulent separated boundary layer and the wake is basically unsteady. The instrumentation employed in the present tests is heavily damped and, therefore, records time-averaged quantities. However, the readings from the five tube probe were repeatable within ±5% even under extreme post-stall conditions.

RESULTS AND DISCUSSIONS

Separation point: Exploration of the point of separation was carried out at angles of attack of 10.3°, 14.4° and 18.4°. Surface flow visualization methods and the tuft spoke survey were found to agree very well with the separation point obtained from the surface pressure distribution. However, the tuft spoke survey did not show realistic depths of separated regions. It is believed that mutual interference of the tufts resulted in magnified depth of the reversed flow regions.

Velocity plots: Computer plots of the velocity profiles at the mid-span section are shown in Figures 2, 3 and 4. Velocity

profiles obtained from flat tube and cylindrical tube are
shown in Figures 5, 6 and 7. While measuring the total pres-
sure values with flat tube and cylindrical tube probes, a prob-
lem was encountered for positions very close to the wall (distances
less than 1.0 mm (.04")). This was attributed to the differential
deflections of the wing and the probe under aerodynamic loads,
similar to those reported in Reference 10. Appropriate correct-
ions have been applied to the present data for these effects,
based upon the method of Reference 10 and special static load
deflection calibrations. The details of these corrections are
given in the Appendix.

The velocity profiles at the point of separation did not
in general exhibit the vertical slope characteristic of separa-
tion profiles. This probably reflects on the capability and
the limitation of the probe. The region near the wall in which
the velocity gradient approaches to zero is very small (about
0.05%c) as indicated by the velocity profiles at one or two
chordwise stations downstream from the separation point. (For
example 90% and 100%c at 10.3°, 75%c at 14.4°, and 60%c at 18.4°.)
Neither of the two probes employed could detect the reversed
flow, thus very shallow regions of separation are indicated.
Surface tufts, on the other hand, very clearly indicate flow
reversal at these stations. At the chordwise station of 100%c
for 10.3° and 18.4° angles of attack, satisfactory total pressure
measurements could not be made either with the flat tube probe
or with the cylindrical tube. This is attributed to very low
velocities (about 5 or 10% of free stream velocity) with violent
fluctuations around the zero velocity point in the region less
than about .05% chord above the surface. The probe interference
might be contributing to the violent fluctuation. In these reg-
ions the indicated dynamic pressure was negative for probe yaw
directions of both 0° and 180°.

Static pressure profiles: Static pressure profiles obtained
from the five tube probe at various chordwise stations on the
airfoil are shown in Figures 8, 9 and 10, together with the
surface static pressures. A close examination of these profiles

reveals distinctly the region of viscous layer characterized
by constant static pressure. The inviscid outer flow region
is indicated by static pressure gradually decreasing toward
the free stream value (c_{p_s} = 0). Thus the general character
of the boundary layer and potential flow fields are clearly
seen, with the exception of some scatter within a height of
about .05% chord at 5% chord station. At this station the
presence of the transition strip caused a rise in the local
static pressure, and influenced the local profile.

Overall static pressure field: Static pressure contours de-
rived from the pressure distributions obtained at ten chordwise
stations on the airfoil and four chordwise stations beyond the
trailing edge (x = 105.6, 110, 120 & 150%c) are shown in Figures
11, 12 and 13. A close look at the wake regions indicates a
distinct high pressure ridge a short distance behind the airfoil.
A relatively steep vertical pressure gradient from lower surface
region to upper surface is also observed indicating a vertical
flow tendency. The velocity plots (Figure 2, 3 and 4) substant-
iate this tendency for upward turning of the lower surface flow.

Boundary layer characteristics: Figures 14 and 15 show the
growth of displacement and momentum thickness on the airfoil,
indicating substantial increases between pre-stall and post-
stall conditions. The shape factor variations at these conditions
are shown in Figure 16. All three curves indicate the character-
istic behavior of the turbulent separated boundary layer, i.e.,
rapid growth prior to separation.

For the case of 18.4° angle of attack, the value of shape
factor at the separation location (45% chord) is 1.67, which
is a little below the theoretical range of 1.8 to 2.2 ordinarily
associated with separation (Reference 11). This discrepancy is
believed to be caused by the fluctuations associated with the
post-stall turbulent flow fields. This results in some fluctua-
tion of the point of separation. However, the value of the

shape factor of 1.8 is seen to be attained at the 47.5% chord
station. Shape factor values for separation points observed
for 10.3° and 14.4° angle of attack (80% and 65% chord) agree
very well with the expected values (Table 1).

TABLE 1 - Shape Factors at Separation

α	Separation Point From Tuft & Pressure Data	Shape Factor H	Normally Expected Value of H
10.3°	80% c	1.92	1.8 to 2.2
14.4°	65% c	1.81	1.8 to 2.2
18.4°	45% c	1.67	1.8 to 2.2

The boundary layer displacement thickness superimposed on
the airfoil is shown in Figure 17. The augmented surface follows
the airfoil surface very closely up to the point of separation
and then diverges away with varying degree of slope depending
on the depth of the separated layer. A similar trend is shown
by the separation streamline, which is obtained by equating
the mass flow in the reversed flow region to that of the flow
in the forward direction. This is plotted for angles of attack
of 14.4° and 18.4° in Figure 18.

Velocity and pressure distribution in the wake: Velocity pro-
files, static, and total pressure profiles are shown in Figures
19 through 21 for a z range of about -8% to 20%c at each chord-
wise station. The progressive growth of the width of the wake
with increasing longitudinal station is seen as expected. Pro-
gressive reduction of static pressure gradients in the wake can
also be seen.

Total pressure profiles at the higher angles of attack
show irregular shapes near the trailing edge, but become progress-
ively smoother downstream. Contour plots of the total pressure
(Figure 22) appear to be basically different between pre- and
post-stall conditions. At 18.4° (post-stall) angle of attack,

9

two low pressure regions can be seen, whereas the 10.3° and
14.4° cases have only one low pressure region.

Reattachment point location in the wake: An examination of the
wake velocities, (Figures 19, 20 and 21) indicates a very
interesting feature. The regions of reversal in the wake term-
inate within a relatively short distance downstream from the
trailing edge. This occurs in the region of high pressure ridge
discussed earlier. A detailed interpolation was carried out in
order to establish the point at which the reversed flow termin-
ates. This point, which is characterized by a single zero
velocity point in the velocity profile, is referred to as the
"reattachment point". Before the determination of the reattach-
ment point, wake vertical centers at various chordwise stations
were obtained by picking out the minimum velocity points from
the velocity profiles (Figure 23).

Since at the reattachment point the static pressure and the
total pressure have the same value, total and static pressure
distributions were drawn along the wake center line (Figure 24).
Unfortunately these comparisons did not result in accurate
reattachment point estimation for the case of 18.4° angle of
attack.

A second scheme for obtaining location of the 18.4° reattach-
ment point is to plot u_x versus x for constant z values. These
curves, as shown in Figure 25, permit easy identification of the
most downstream point at which reversed flow (negative u_x) is
present. A summary of reattachment point locations is given in
Table 2.

TABLE 2   Reattachment Point Location

Angle of Attack	Reattachment Point
10.3°	103% c
14.4°	106% c
18.4°	117% c

10

Integrated boundary layer characteristics of the wake: The
boundary layer characteristics of the wake depend on the
free shear layer generated at both top and bottom separations
from the airfoil surface. The wall shear stress, of course,
vanishes in the wake. For flow situations where the wake is
symmetric, numerical integration can be carried out for the
top or bottom half of the wake alone. In such cases the
entrainment of mass from the upper and lower jet sheets would
be equal.

When the wake is asymmetric as in the present case, the
entrainments of mass by the upper and lower jet sheets are
no longer equal. Since mass is transferred between the upper
and lower streams, it is not possible to distinguish upper
side displacement or momentum thicknesses aft of the trailing
edge. Consequently, estimation of the dividing streamline
between the wake jet sheets generated by the airfoil upper
and lower surfaces is not possible. Also, the recirculation
region, which terminates at the reattachment point, is charac-
terized by relatively strong vertical and horizontal pressure
gradients (Figs. 23 through 25). Vertical pressure gradients
violate the underlying assumptions of Von Karman's momentum
integral approach (Ref. 11).

For the reasons just outlined, the integrated boundary
layer characteristics of the wake are difficult to assess.
In any case, they should be expressed in terms of total width
of the wake.

Unfortunately, in the present research, measurement were
not obtained to the lower edge of the wake viscous region
because of the limitations of the stroke of the probe travers-
ing mechanism. Thus, even though the outer edge of the viscous
region of the upper surface wake was surveyed, calculations of
longitudinal variations of the displacement thickness, momentum
thickness and the separation streamline were not carried out
for positions downstream from the trailing edge.

11

Skin friction computations: Several attempts were made to obtain the skin friction distribution up to the point of separation, employing the Von Karman momentum integral approach (Reference 11). The results were not consistent, expecially near 5% and 10% chord stations, where the velocity gradients are steep and momentum thicknesses are small. These discrepancies are attributed to inaccurate estimation of velocity and momentum thickness gradients with relatively few data points. Experimental methods like the Preston tube and razor blade techniques (References 12 & 13) should be exploited in measuring the local skin friction, especially in the region of rather large pressure gradients. Also, the possibility should be explored of using these techniques under separated flow conditions, where the velocity gradients are low.

CONCLUSIONS

1. Experimental velocity profiles, flow inclinations and static pressure distributions have been obtained for the GA(W)-1 airfoil upper surface and wake at typical pre- and post-stall angle of attack conditions. The data include reversed flow regions of separated boundary layers.

2. Integrations of velocity profiles to obtain displacement thickness, momentum thickness and the separation streamline show that all of these parameters exhibit a rather steep diverging trend from the separation point to the airfoil trailing edge.

3. The present tests reveal that the region of reversed flow associated with separation terminates at a reattachment point which is located a short distance downstream from the airfoil trailing edge.

4. Attempts to determine skin friction distributions by
    indirect methods did not result in meaningful values.

RECOMMENDATIONS

1. Boundary layer characteristics on the airfoil lower
    surface and outer edge of the associated viscous
    region of the wake should be obtained. These will aid
    in establishing meaningful mathematical models for
    separated flows.

2. More direct methods for measurement of local skin friction
    employing the Preston tube or razor blade should be employ-
    ed as possible means for obtaining skin friction distrib-
    utions.

3. A rather detailed scanning of the wake at closer chordwise
    intervals should be obtained in order to refine the
    interpolated reattachment point location obtained from the
    current series of experiments.

4. The experimental techniques utilized in the present research
    should be applied to an airfoil-flap combination to determine
    the important features of separated flows with multi-element
    configurations.

Aeronautical Engineering Department
  Wichita State University
    Wichita, Kansas 67208
      December 1974

REFERENCES

1. Liebeck, R. H.: A Class of Airfoils Designed for
    High Lift in Incompressible Flow. AIAA Paper 73-86,
    January 1973.

2. Stevens, W. A., Goradia, S. H.; and Braden, J. A.:
    Mathematical Model for Two-Dimensional Multi-
    Component Airfoil in Viscous Flow. NASA CR-1843,
    July 1971.

3. Bhateley, I. C.; and McWhirter, J. W.: Development of
    Theoretical Method for Two-Dimensional Multi-element
    Airfoil Analysis and Design. Part 1 - Viscous Flow
    Analysis Method, AFFDL-TR-73-96, August 1972.

4. Hahn, M.; Rubbert, P. E.; and Mahal, A. S.: Evaluation
    of Separation Criteria and Their Application to
    Separated Flow Analysis. AFFDL-TR-72-145, January 1973.

5. Kuhn, G. D.; and Nielsen, J. N.: Prediction of Turbulent
    Separated Boundary Layer. AIAA Paper 73-663, July 1973.

6. Mechtley, E. A.: The International System of Units -
    Physical Constants and Conversion Factors (Revised)
    NASA SP-7012, 1969.

7.. Wentz, W. H., Jr.; and Seetharam, H. C.: Development of
    a Fowler Flap System for A High Performance General
    Aviation Airfoil. NASA CR-2443, December 1974.

8. Braslow, A. L.; and Knox, E. C.: Simplified Method for
    Determination of Critical Height of Distributed Rough-
    ness Particles for Boundary Layer Transition at Mach
    Numbers from 0-5. NACA TN-4363, 1958.

9. Walker, J. K.: Calibration of a Five-Tube Probe. WSU
    AR 74-1, April 1974.

10. Peterson, J. B., Jr.: Boundary-Layer Velocity Profiles
    Downstream of Three-Dimensional Transition Trips on a
    Flat-Plate at Mach 3 and 4. NASA TN-D-5523, 1969.

11. Schlichting, H.: Boundary Layer Theory, McGraw-Hill
    Co., 4th Edition, 1962.

12. Patel, V. C.: Calibration of the Preston Tube and
    Limitations on Its Use in Pressure Gradients,
    J. Fluid Mechanics 23, 1965.

13. East, L. F.: Measurement of Skin Friction at Low
    Subsonic Speeds by the Razor-Blade Technique,
    British R & M 3525.

Probe Wind Shield

Probe Extension

3.175mm

16

Tip Details

Flatten End

1.22mm

.1mm

.15mm

Flat Tube Probe

90° 30°

.45mm

2.54mm

Five Tube Probe

.46mm

.3 mm

.38mm
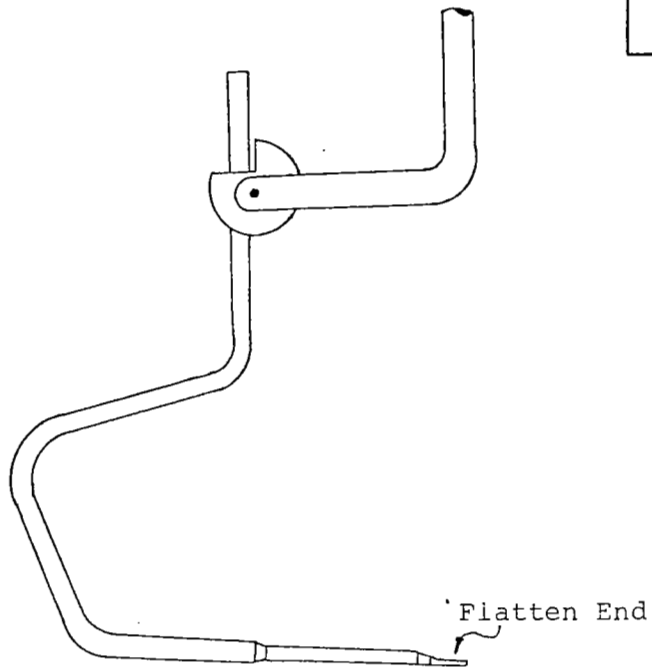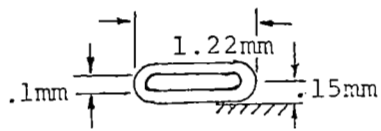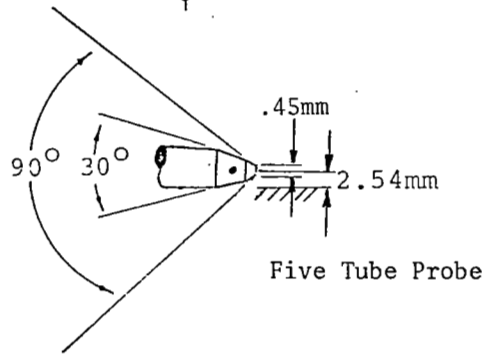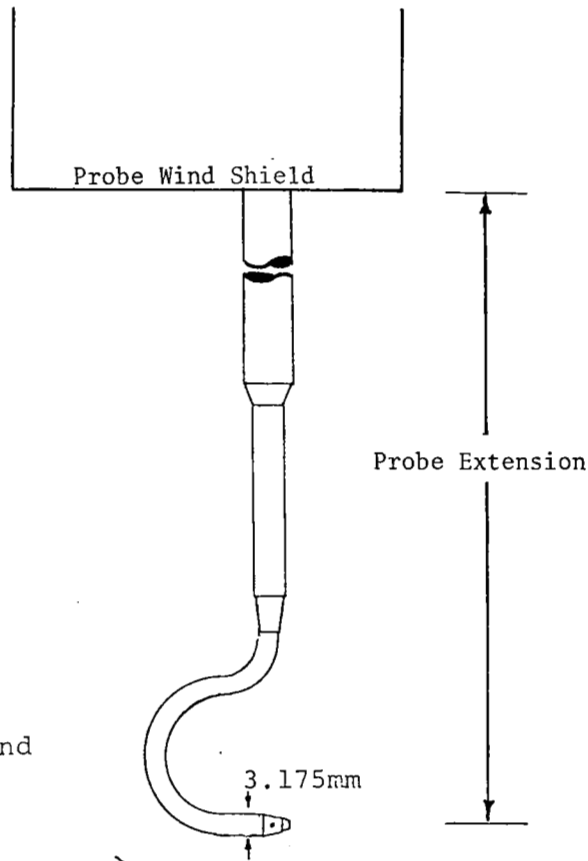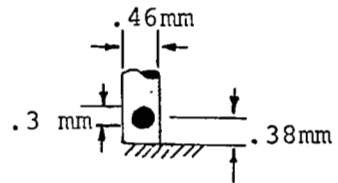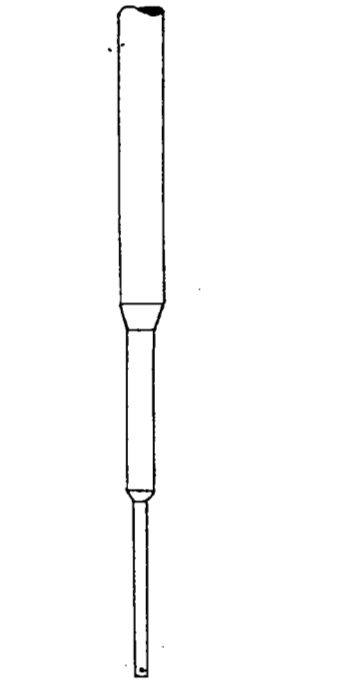
Cylindrical Tube Probe

Figure 1 - Probes

GA(W)-1 AIRFOIL

RN: 2.2×10^6
Mach No.: 0.13
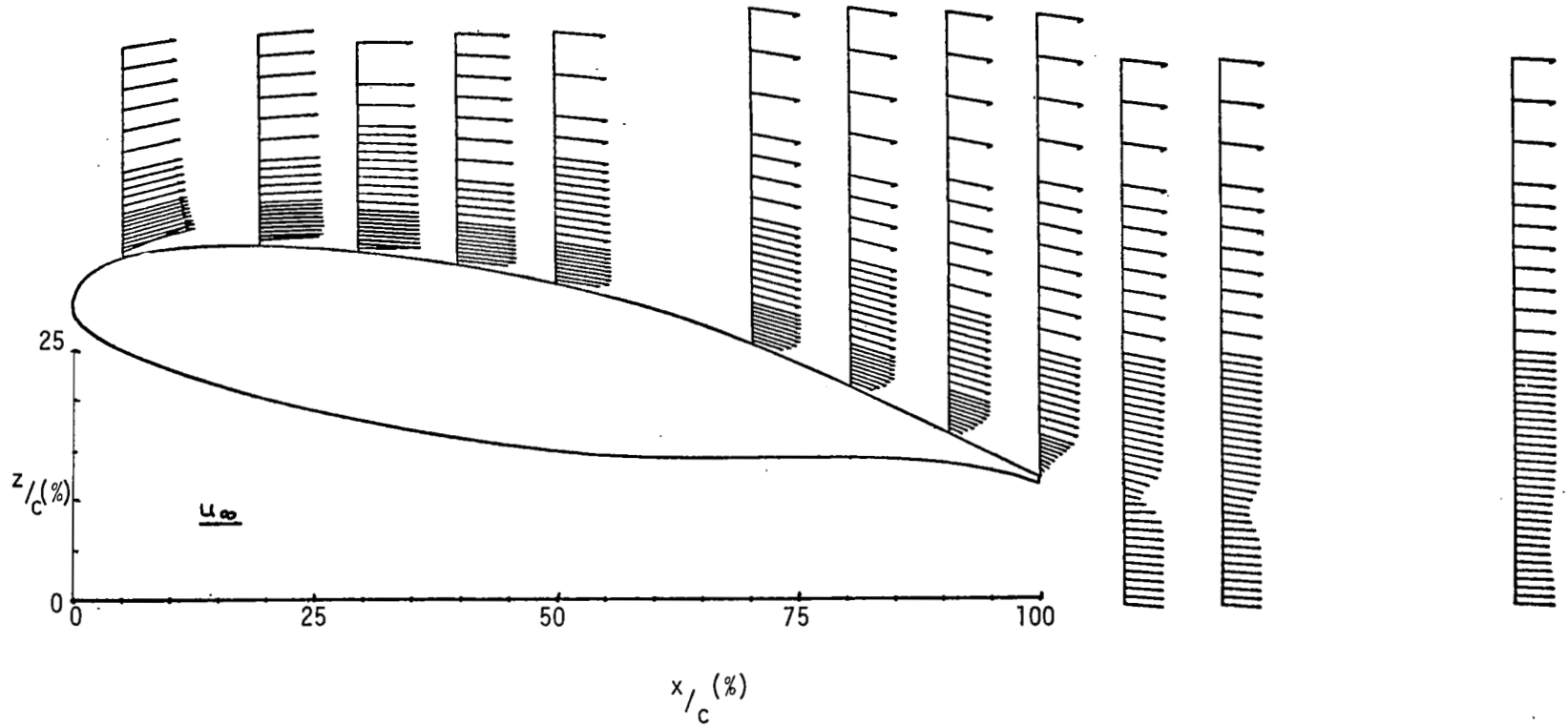
Figure 2 - Experimental Velocity Plot, α = 10.3°

GA(W)-1 AIRFOIL

u_∞
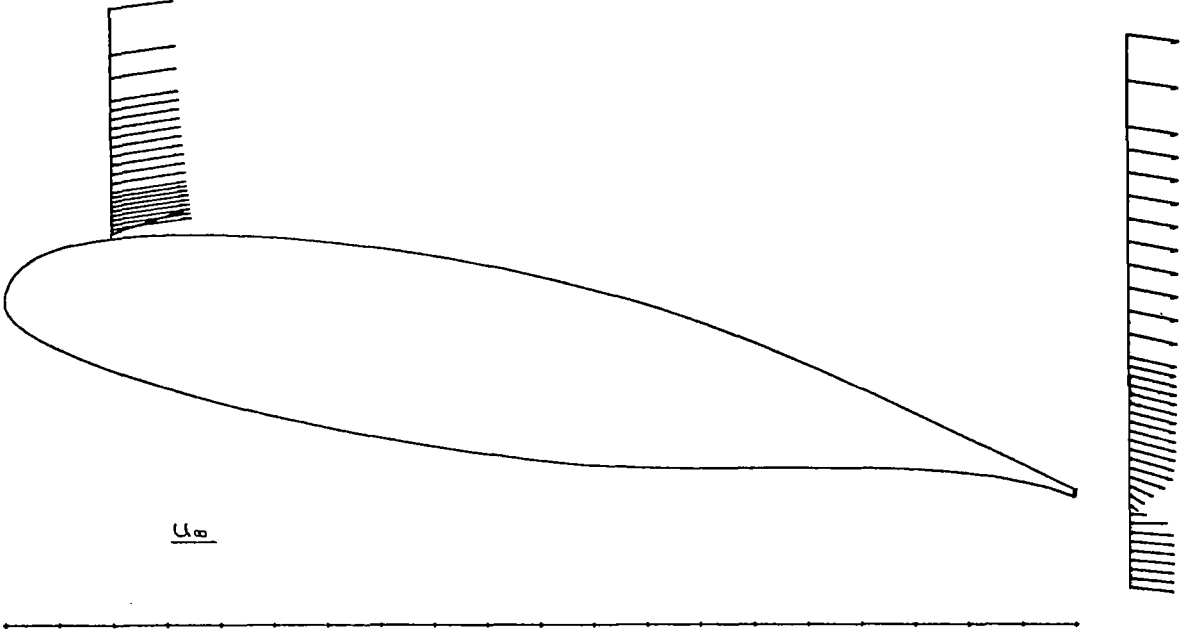
Figure 2 - Concluded

GA(W)-1 AIRFOIL
RN: 2.2x10⁶
Mach No.: 0.13

u_∞
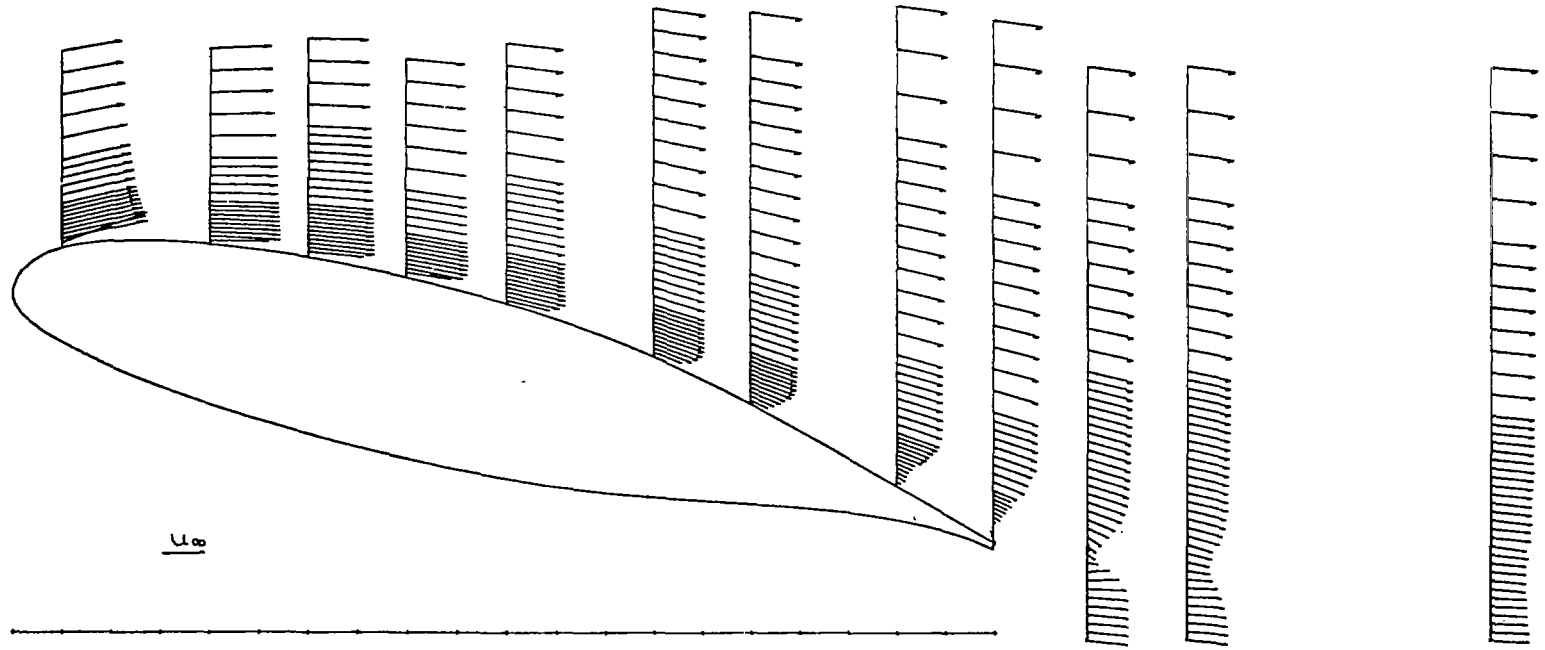
Figure 3 - Experimental Velocity Plot, α = 14.4°

GA(W)-1 AIRFOIL

$\underline{u_\infty}$
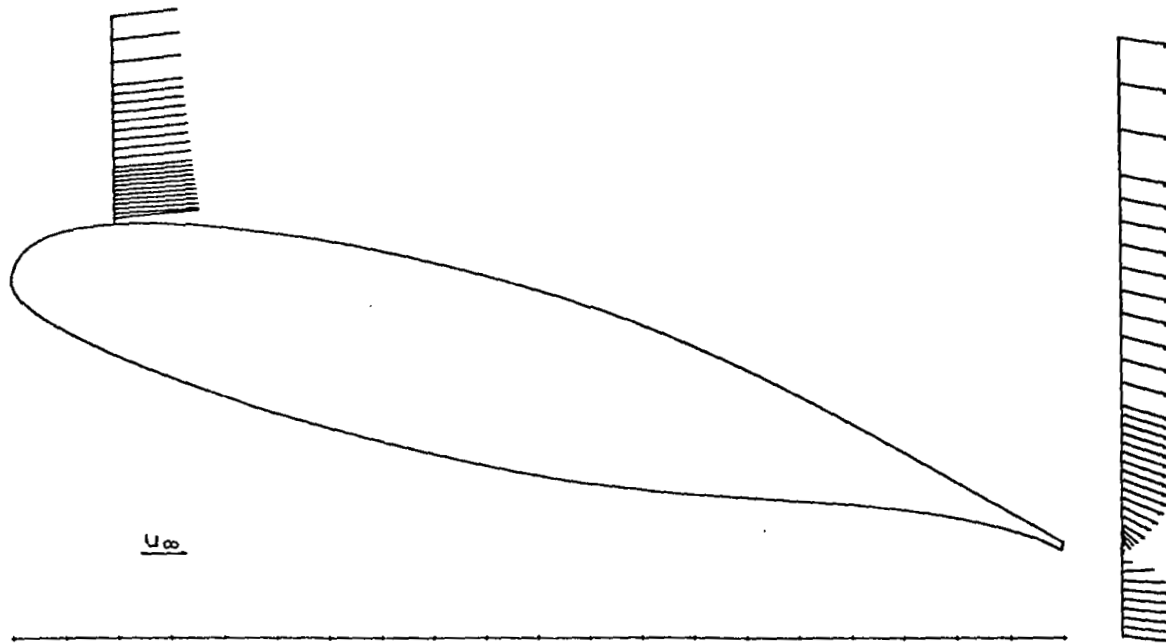
Figure 3 - Concluded

GA(W)-1 AIRFOIL

RN: 2.2×10^6

Mach No.: 0.13

$\underline{u_\infty}$
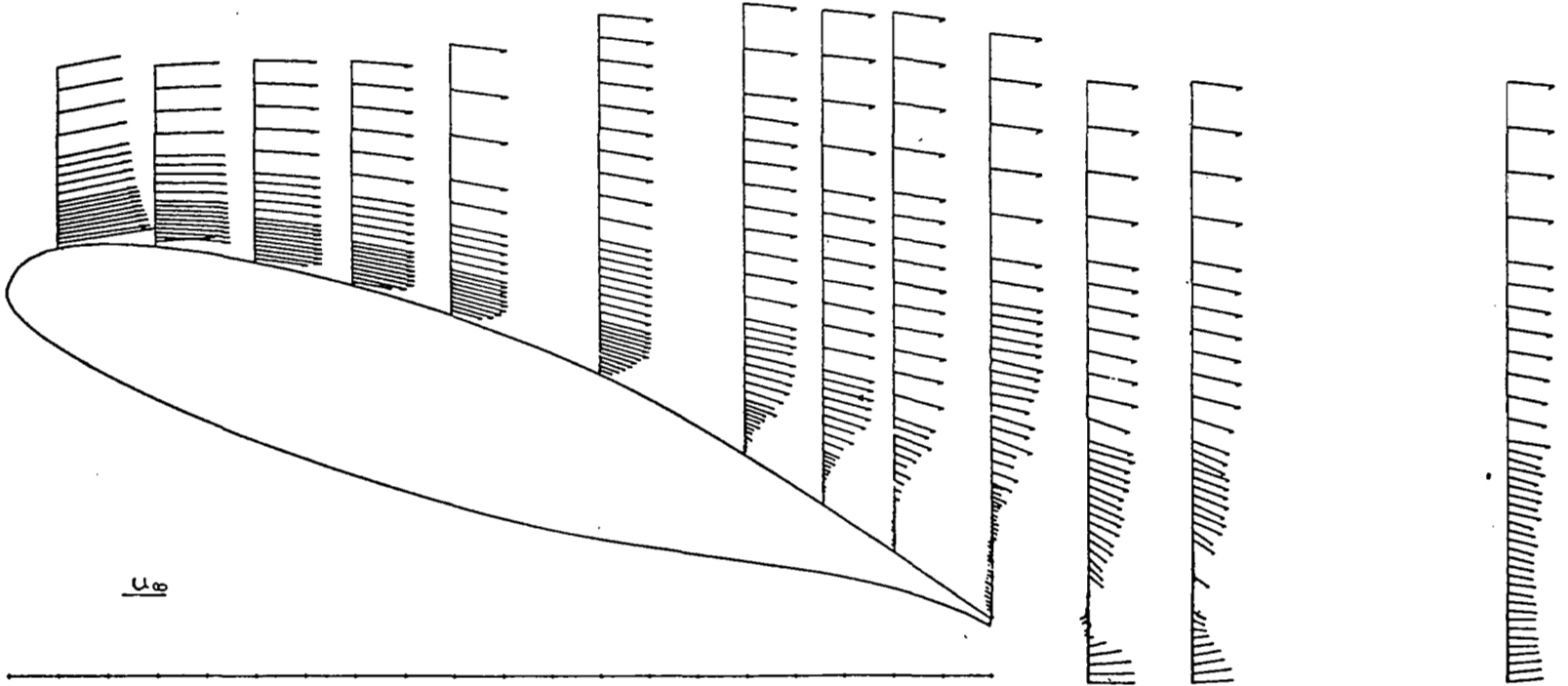
Figure 4 - Experimental Velocity Plot, $\alpha = 18.4°$

GA(W)-1 AIRFOIL

U_∞

Figure 4 - Concluded

I

Cylindrical Probe
Five Tube Probe
Unprimed: Flat Tube Probe

Symbol	$^x/_c$ (%)
⊙	5
⊡	10
◇	20
△	30
◹	40
◿	50
◠	70
◇	80
◇	90

$^z/_c$ (%)

u_x
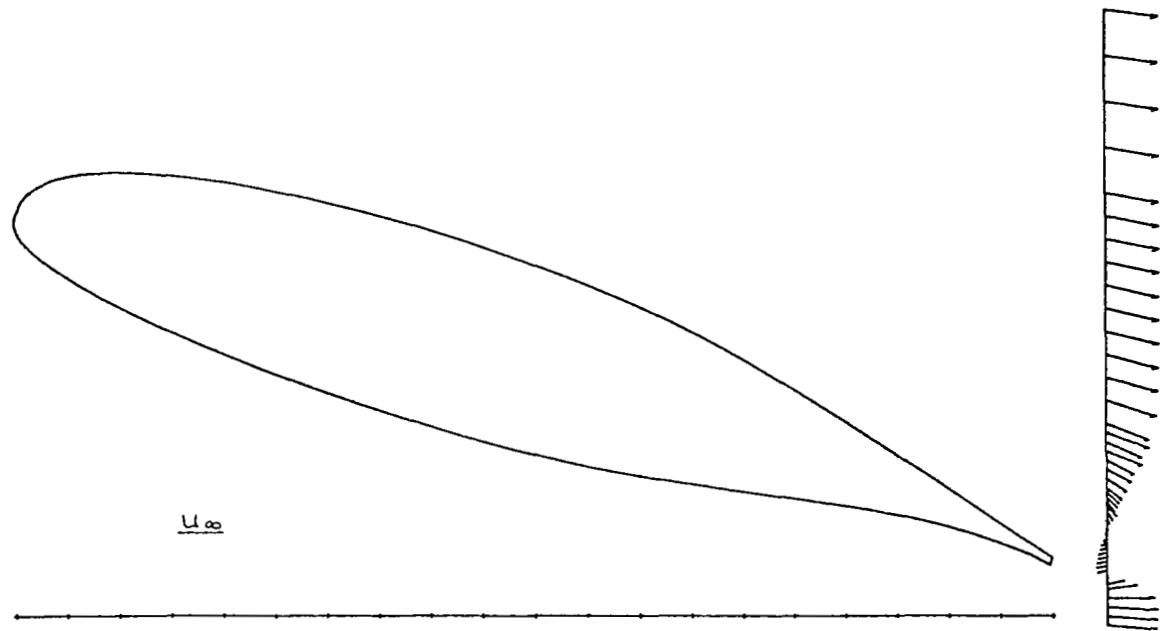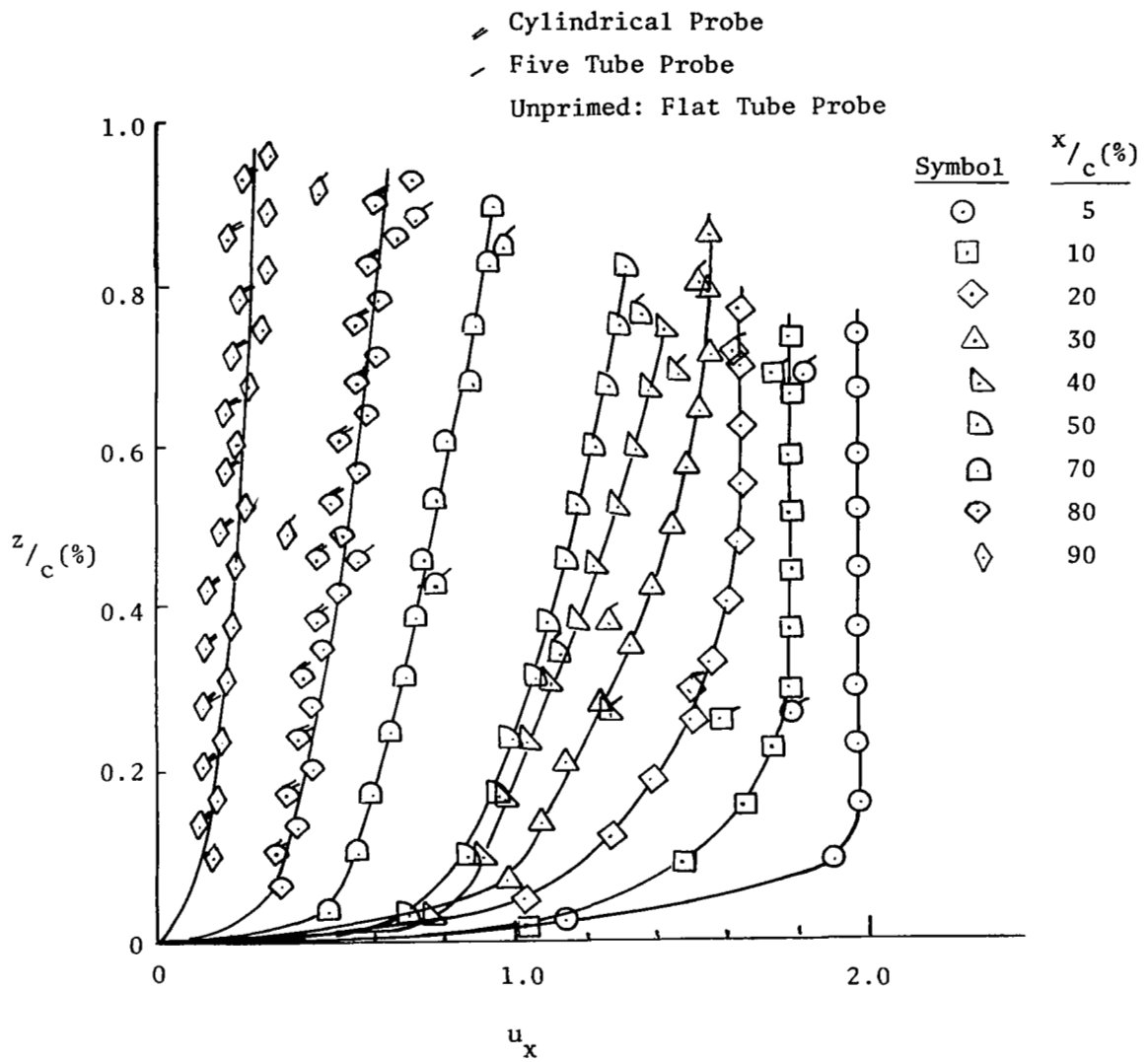
Figure 5 - Near-Wall Velocity Profiles, $\alpha = 10.3°$

23

Symbol	x/c (%)
☉	5
⊡	10
◇	20
△	30
▷	40
◁	50
⌂	65
◇	75
◊	90
⌂	100

⟋ Cylindrical Probe

⟋ Five Tube Probe

Unprimed: Flat Tube Probe
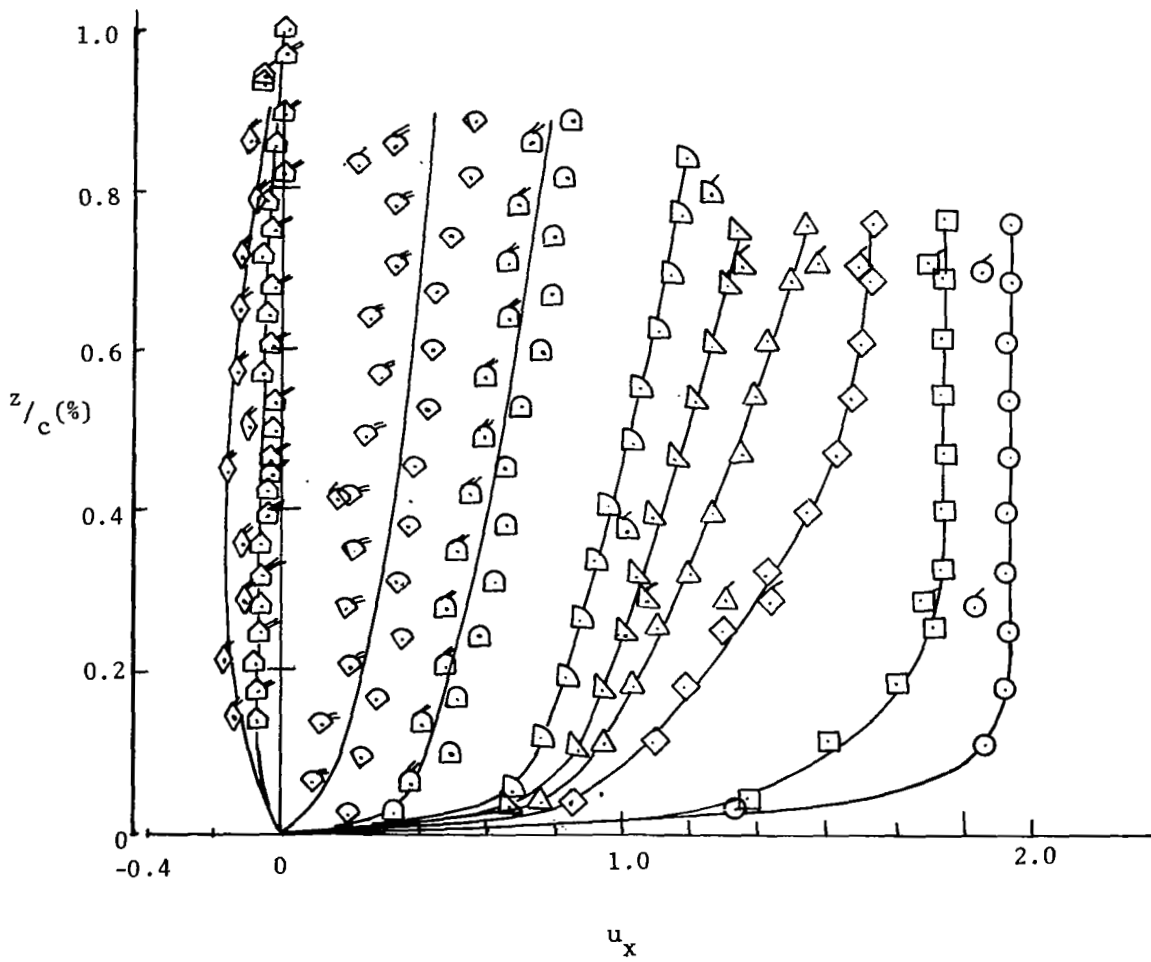
Figure 6 - Near-Wall Velocity Profiles, $\alpha = 14.4°$

Cylindrical Tube

Five Tube Probe

Unprimed: Flat Tube Probe

Symbol	x/c (%)
⊙	5
⊡	15
◇	25
△	35
▷	45
◁	60
⬠	75
◇	82.5
◇	90

z/c (%)

u_x
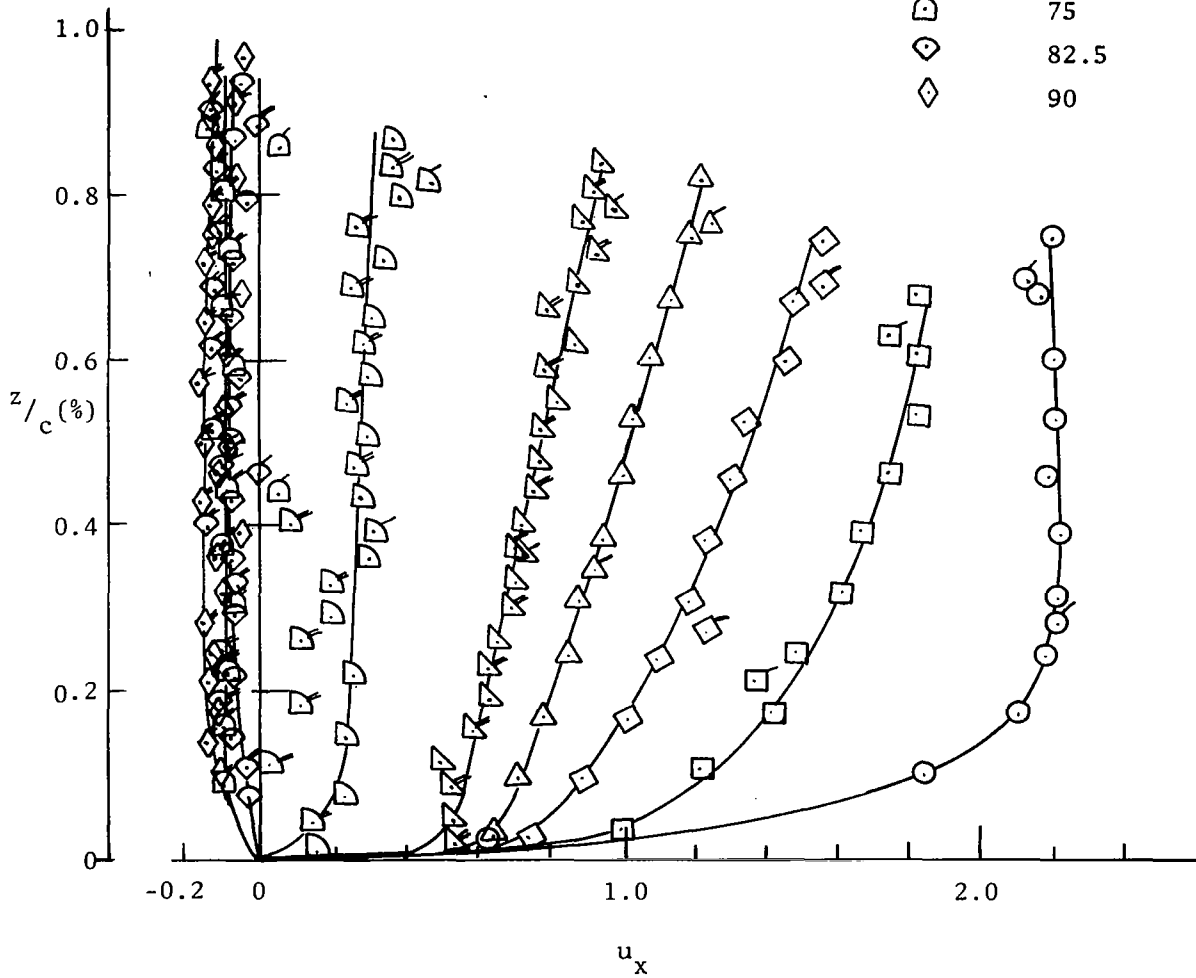
Figure 7 - Near-Wall Velocity Profiles, $\alpha = 18.4°$

Symbol	$x/_c$ (%)
⊙	5
▢	10
◇	20
△	30
◺	40
◿	50
⌂	70
◇	80
◇	90
⬠	100
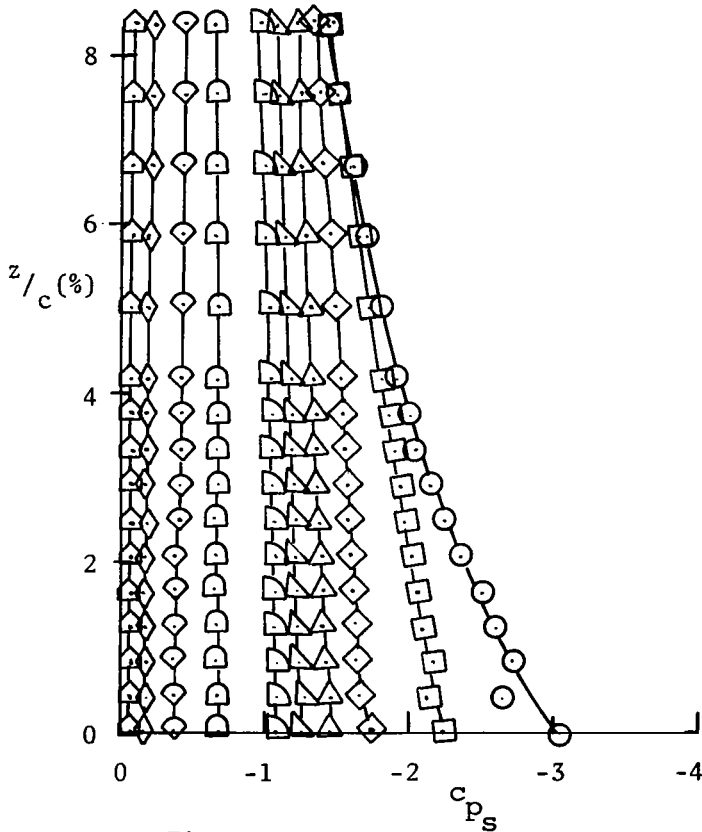
Figure 8 - Static Pressure Profiles, $\alpha = 10.3°$
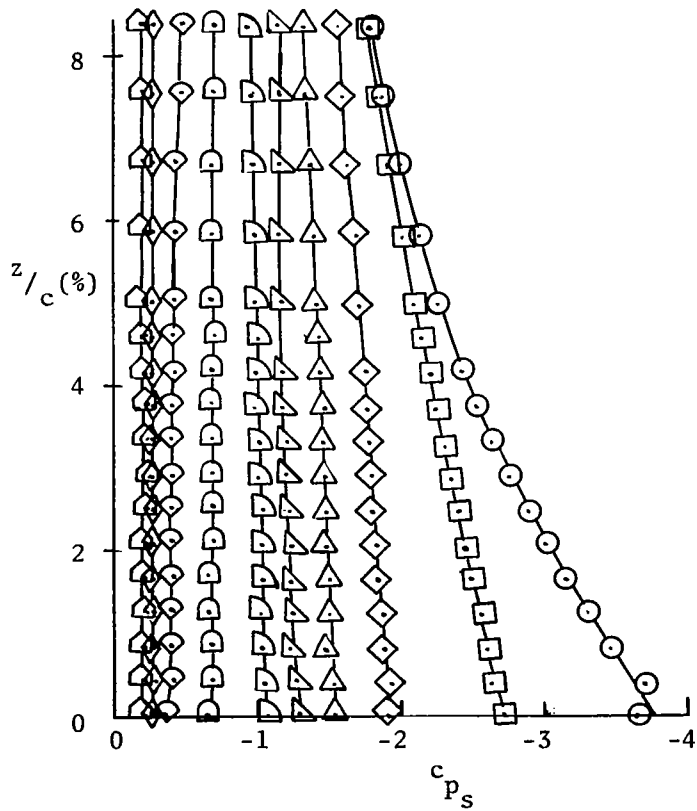
Figure 9 - Static Pressure Profiles, α = 14.4°
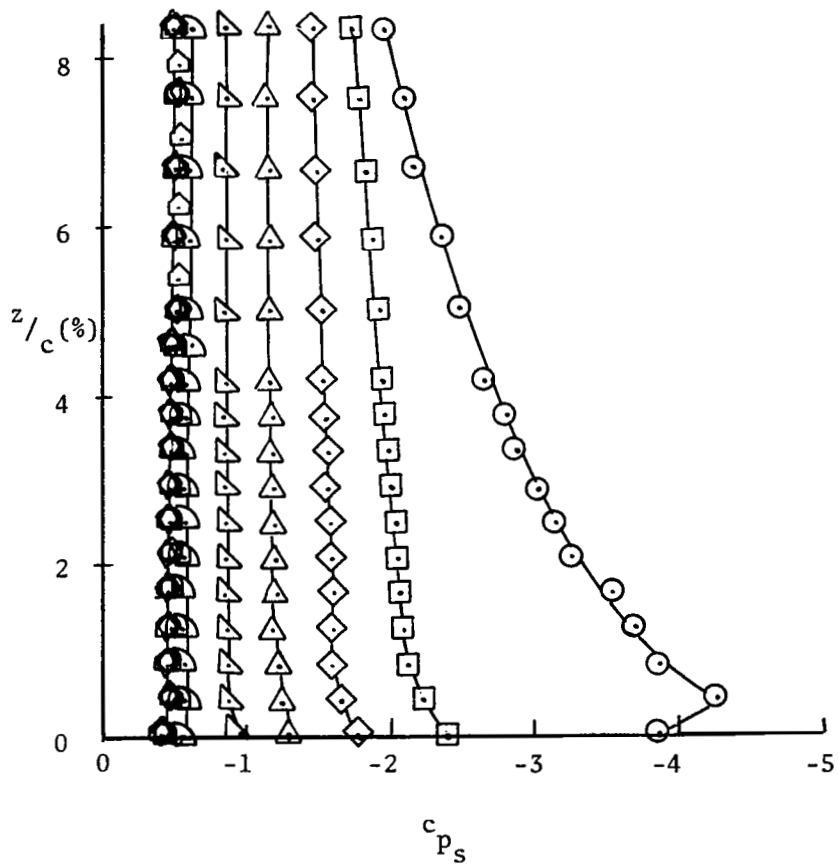
Figure 10 - Static Pressure Profiles, $\alpha = 18.4°$

-1.25 -1.0

-1.5

-0.75 -0.5 -0.4 -0.3

$c_{p_s}=-0.2$

-0.1

-1.75

-2.0

-2.25

-0.075

-0.10

0

-0.005

-0.05

+0.025

-0.025

0 -0.005
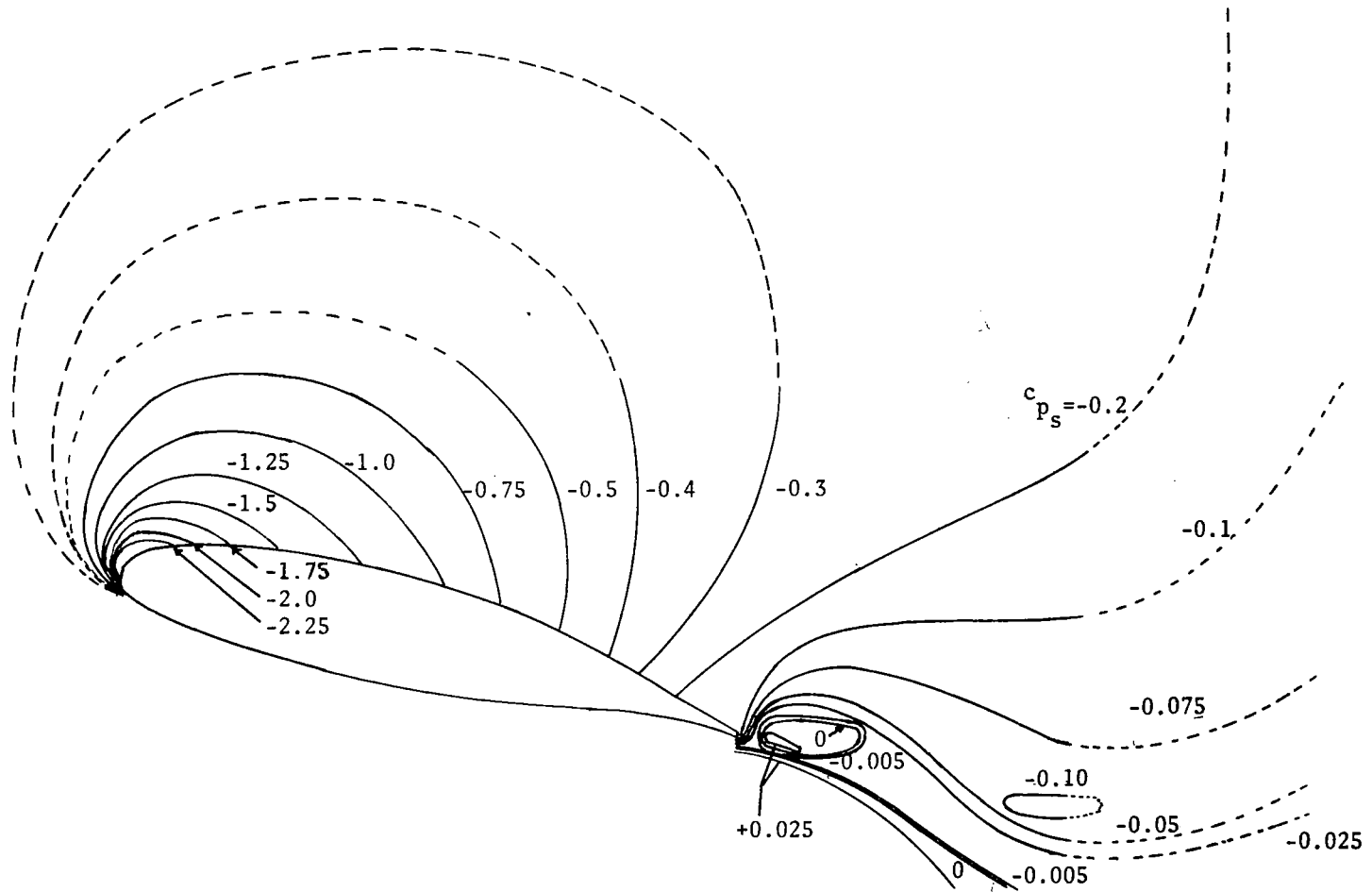
Figure 11 - Static Pressure Field Contours, $\alpha = 10.3°$
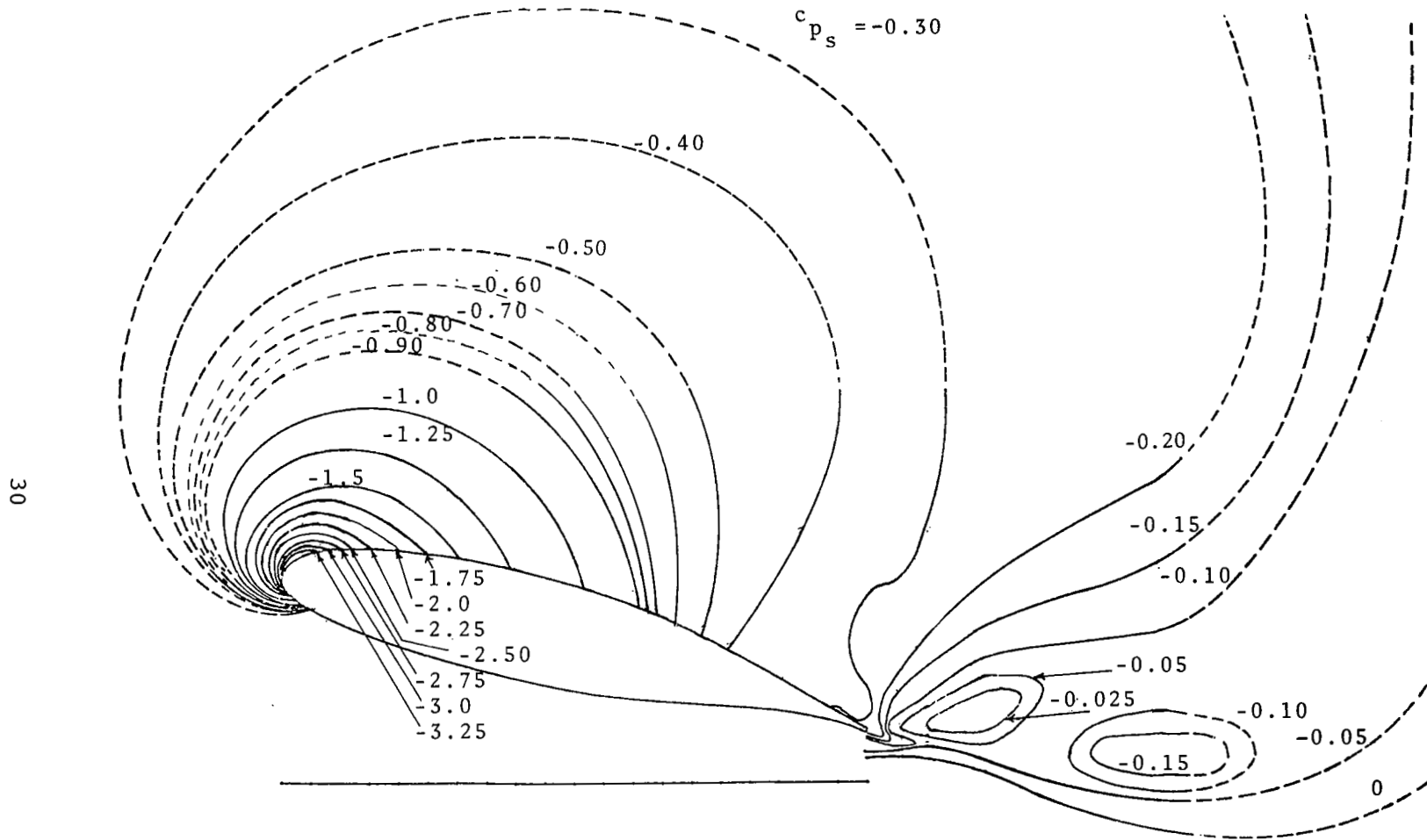
Figure 12 - Static Pressure Field Contours, $\alpha = 14.4°$

$c_{p_s} =$ −3.0

−2.75

−2.5

−2.0
−1.75
−1.5
−1.25
−1.0
−0.9
−0.8
−0.7
−0.6

−0.55
−0.5
−0.45
−0.40
−0.35

−0.25
−0.25
−0.2

−0.2
−0.15
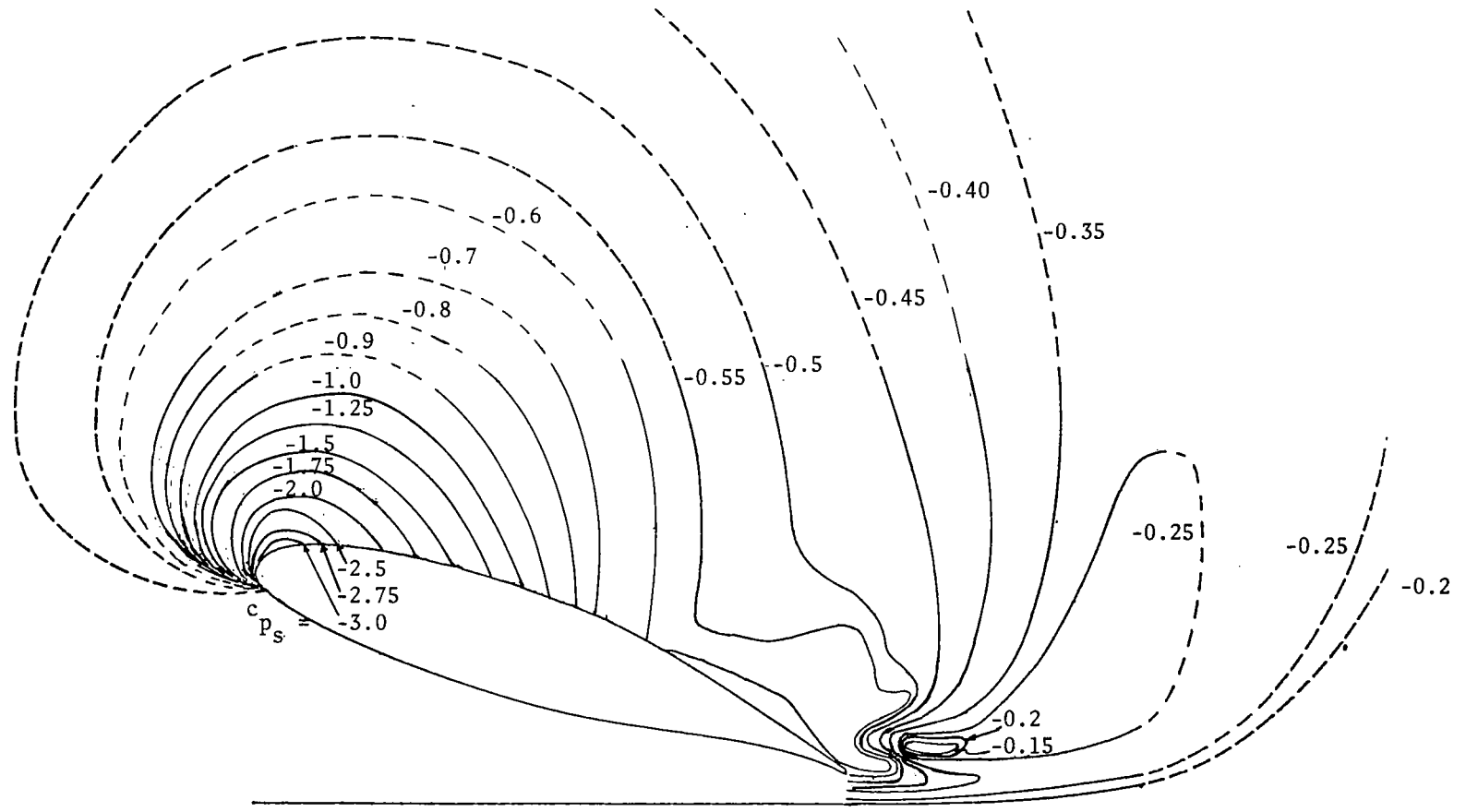
Figure 13 - Static Pressure Field Contours, $\alpha = 18.4°$
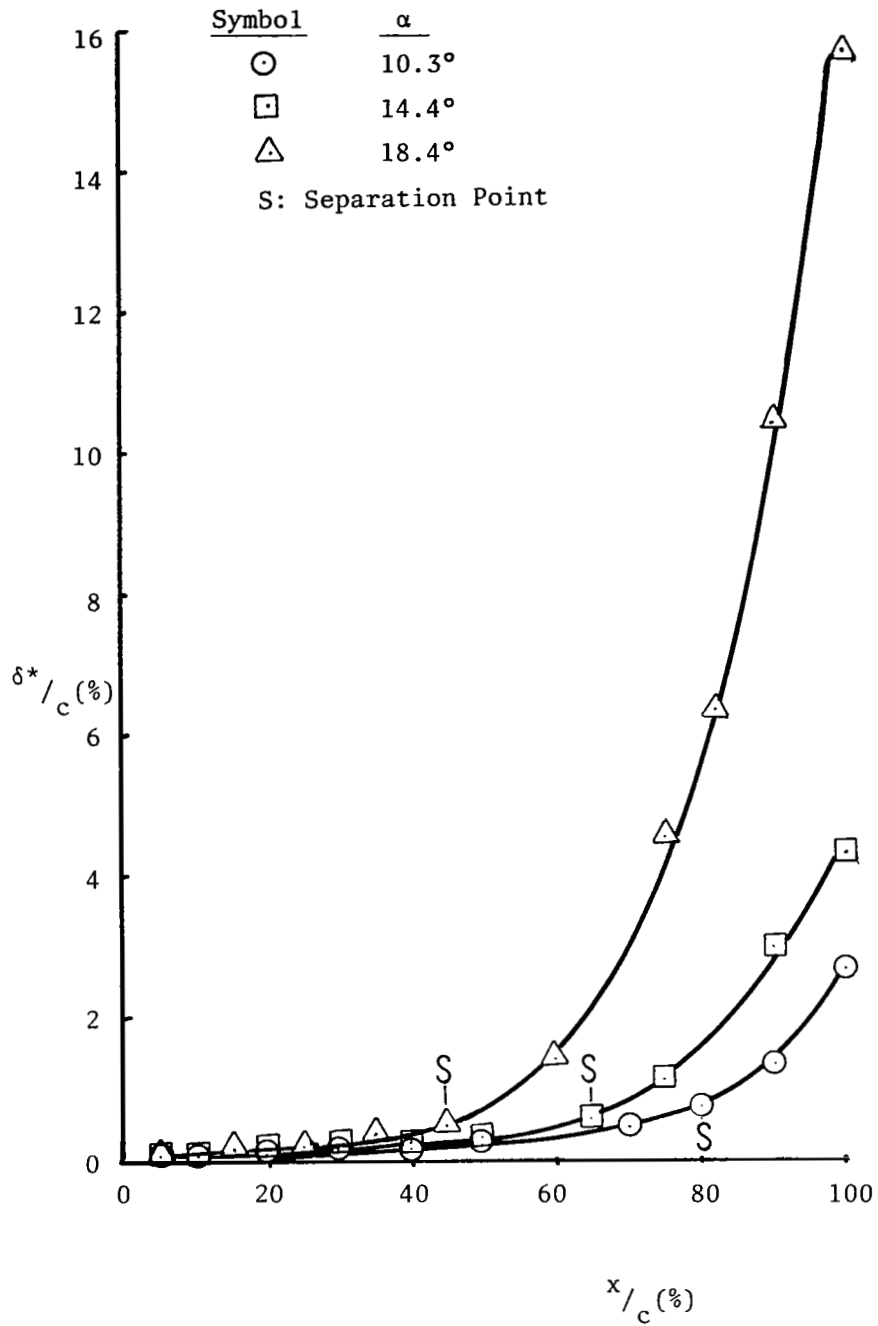
Figure 14 - Boundary Layer Displacement Thickness

32
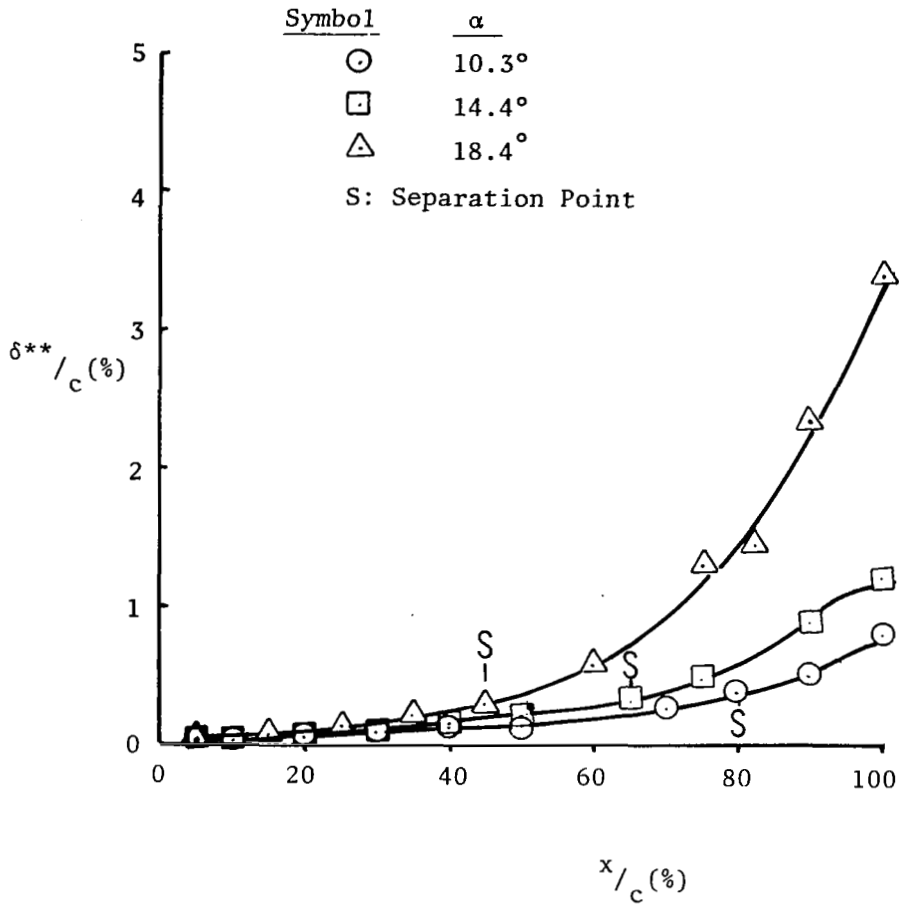
Figure 15 - Boundary Layer Momentum Thickness
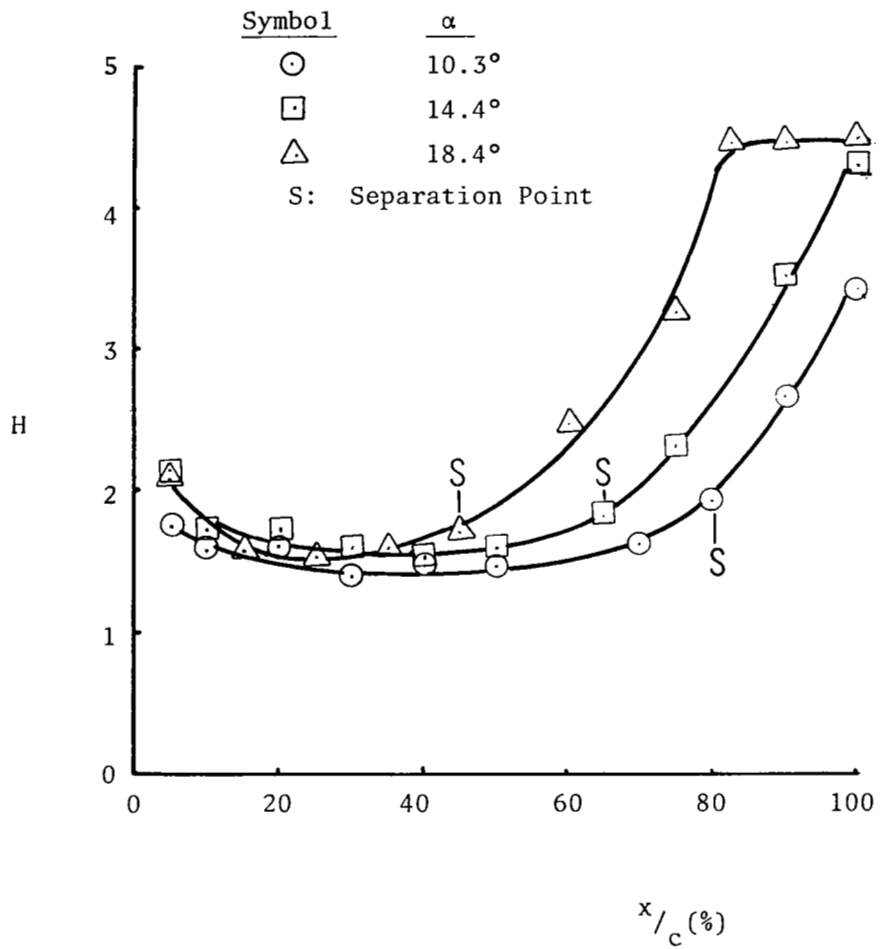
Figure 16 - Boundary Layer Shape Factor

DISPLACEMENT THICKNESS DISTRIBUTION

$$\alpha = 10.3°$$
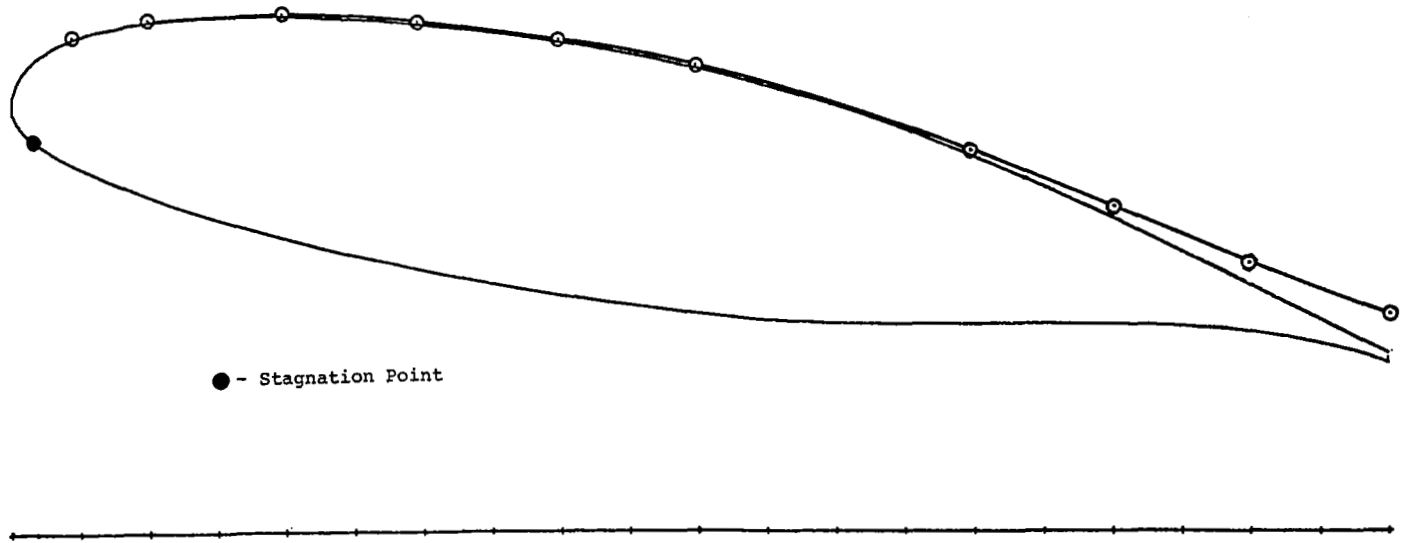
● - Stagnation Point

Figure 17 - Augmented Airfoil Profile

DISPLACEMENT THICKNESS DISTRIBUTION

$$\alpha = 14.4°$$
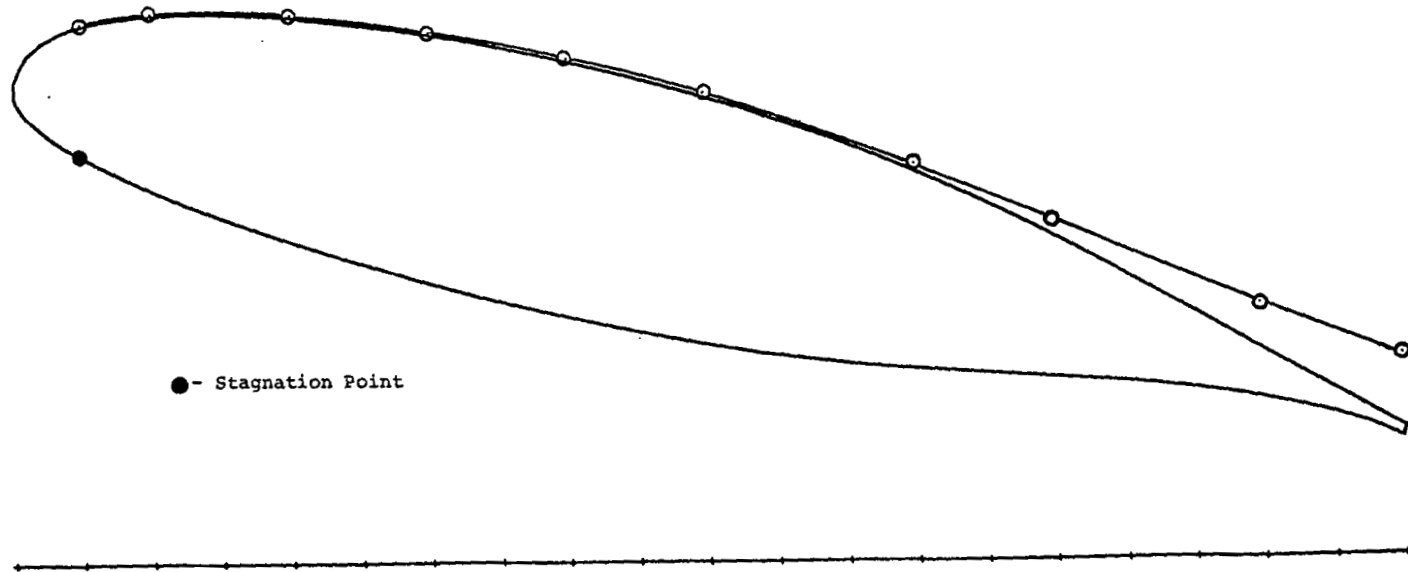
●- Stagnation Point

Figure 17 - Continued

DISPLACEMENT THICKNESS DISTRIBUTION

$$\alpha = 18.4°$$

● - Stagnation Point
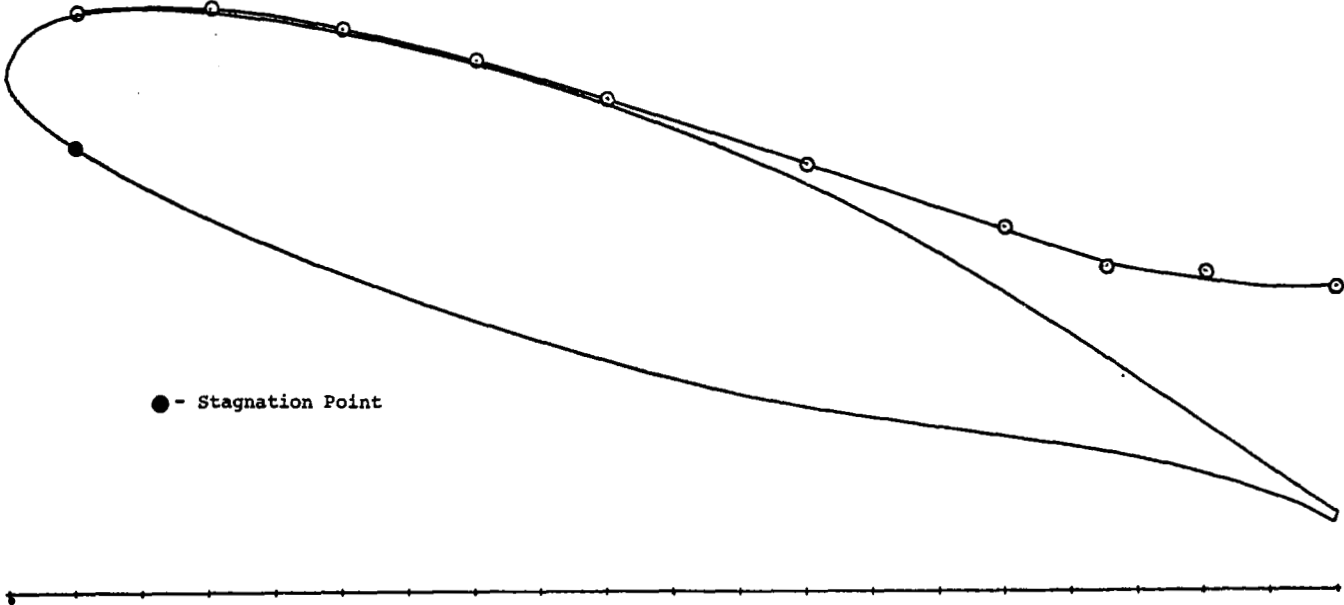
Figure 17 - Concluded
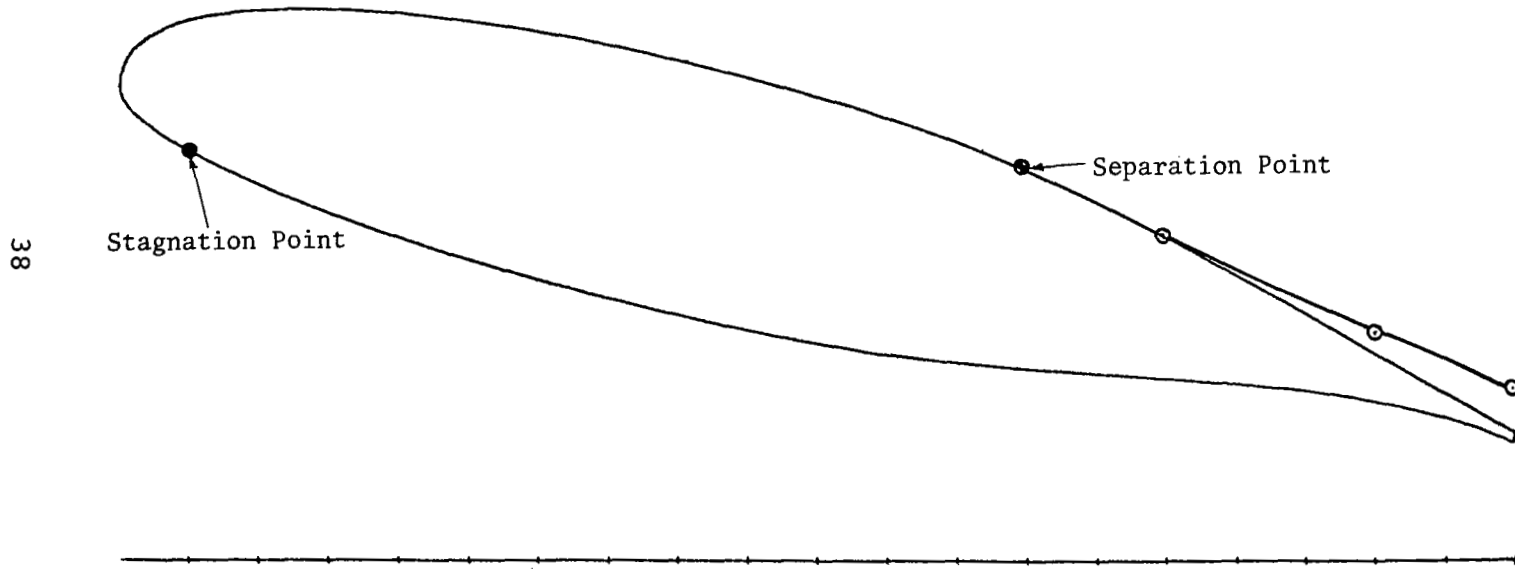
Figure 18 - Separation Streamline
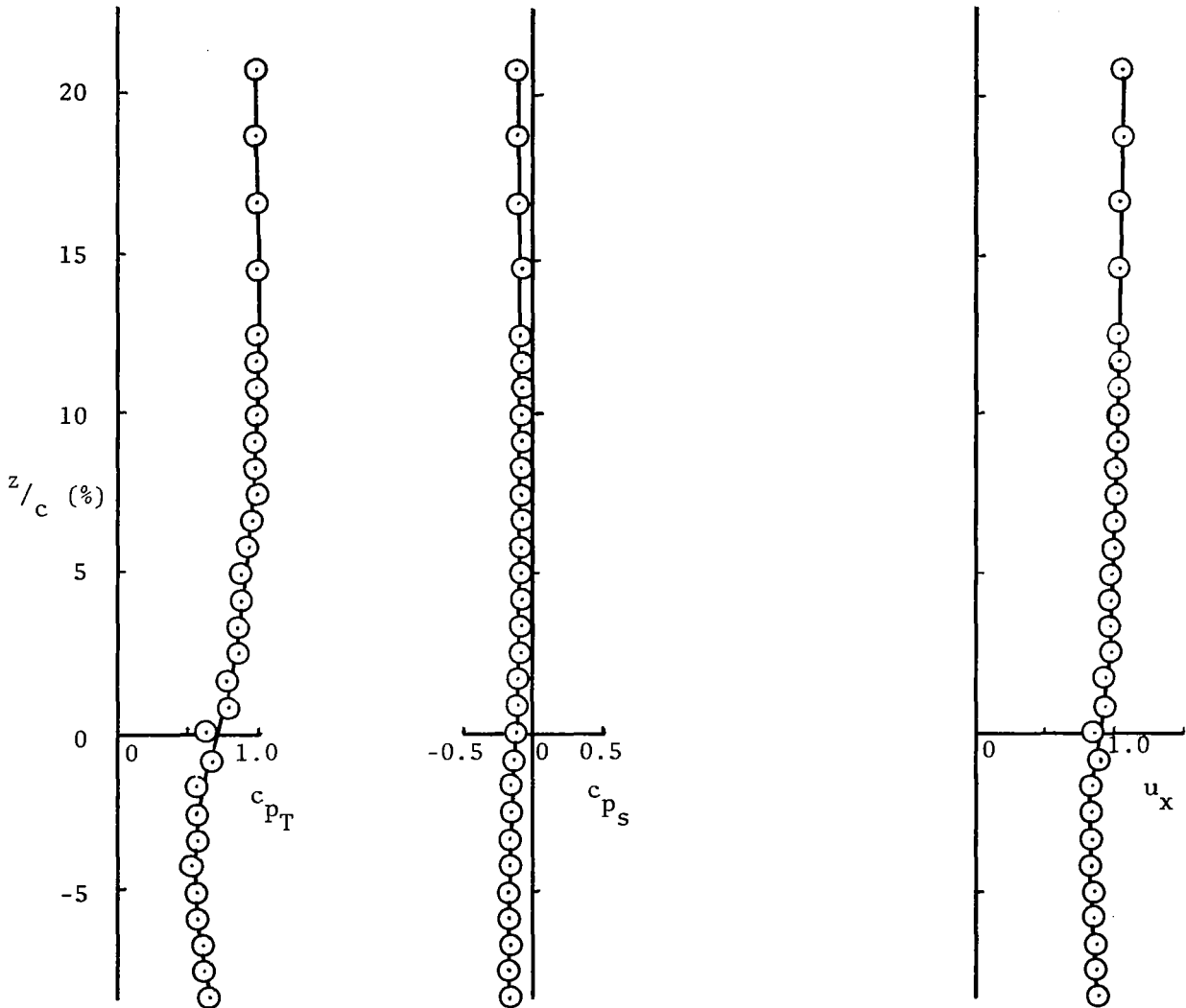
α = 18.4°

Separation Point

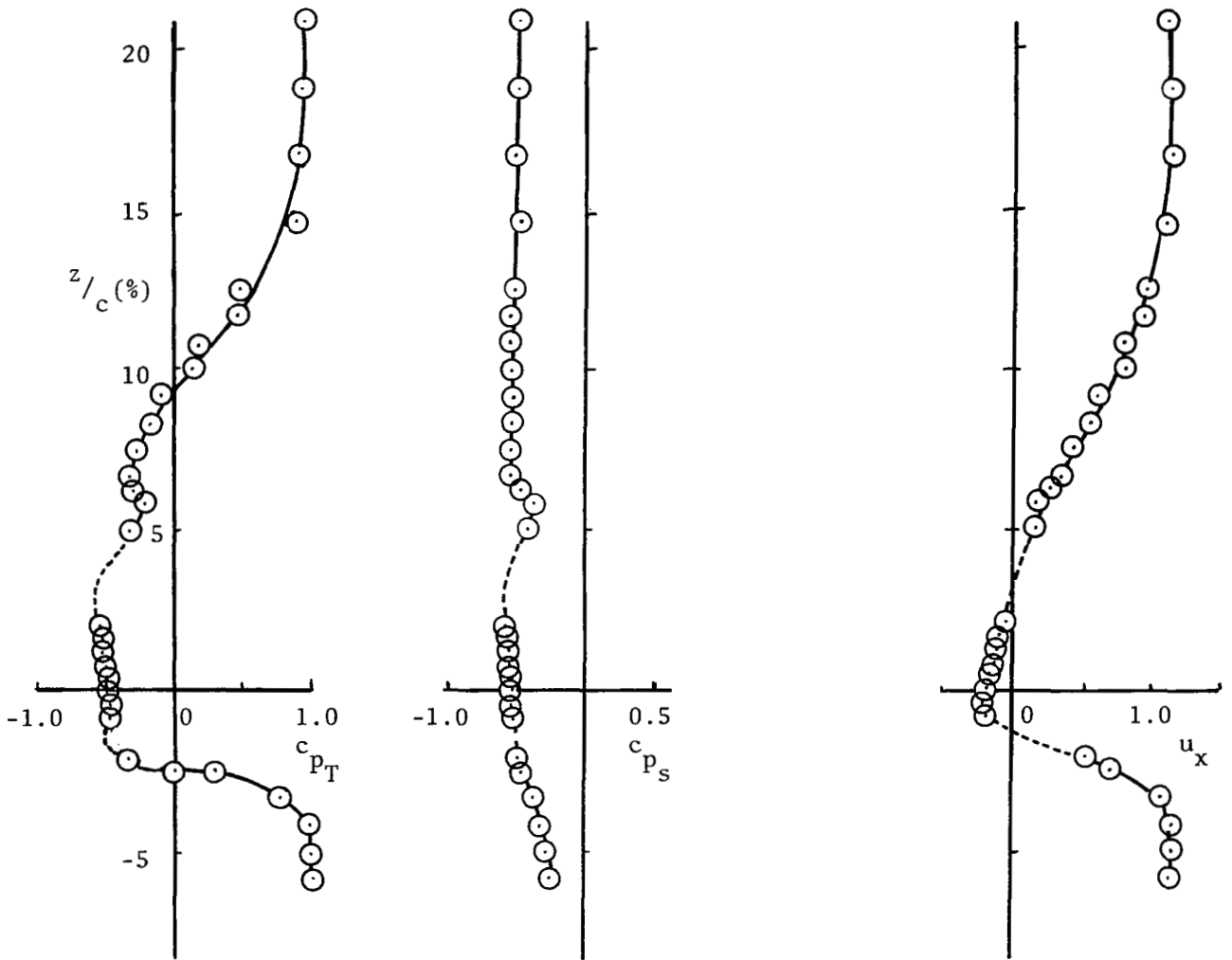Stagnation Point
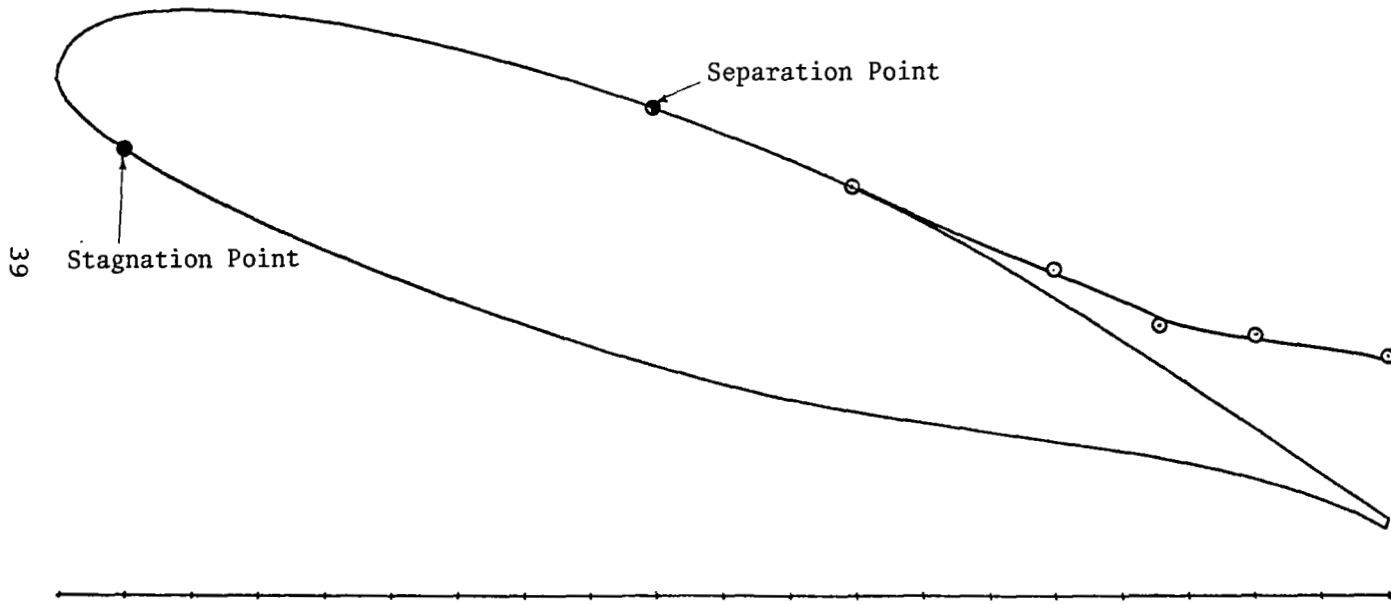
Figure 18 - Concluded.

x = 105.6% c
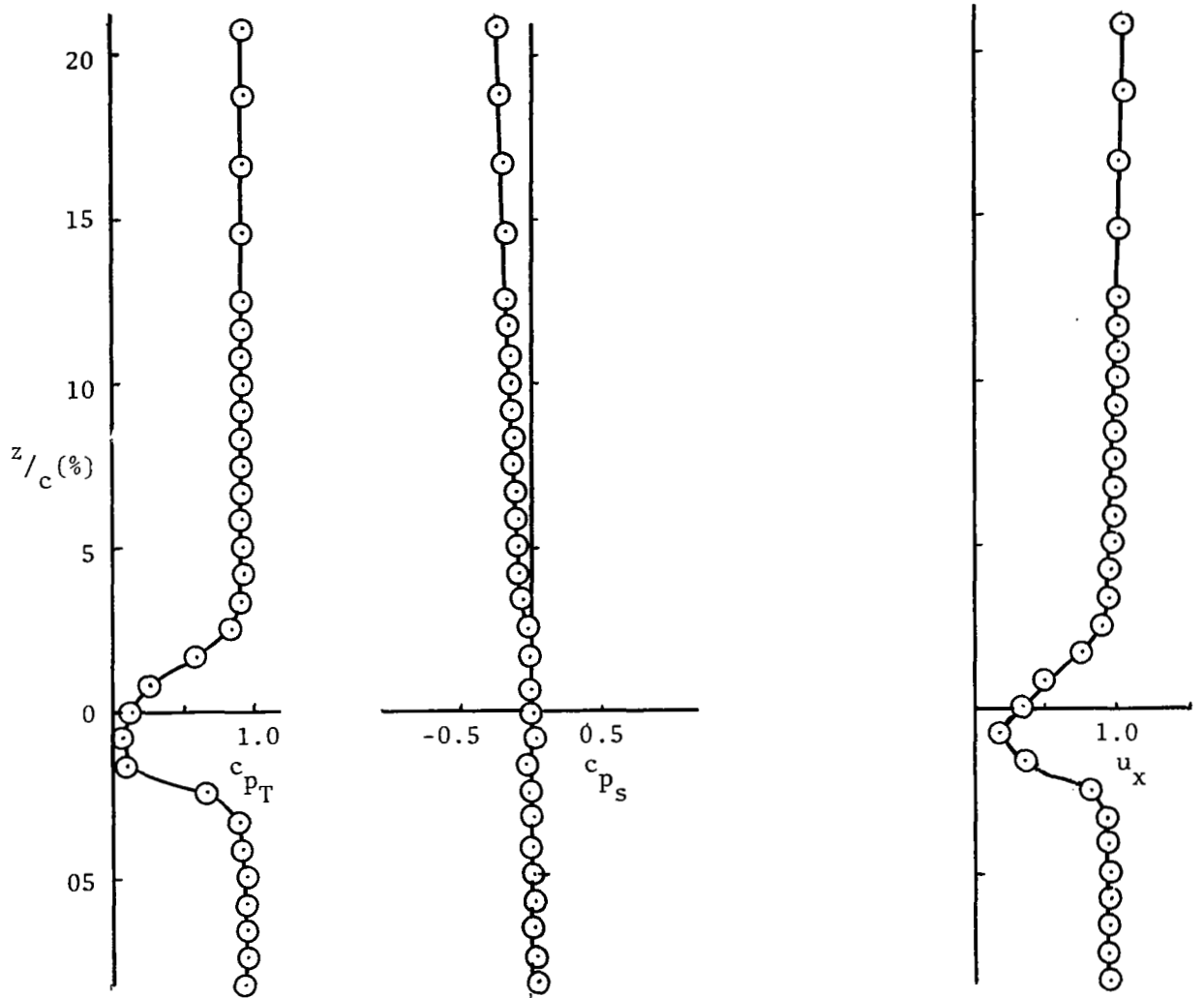
Figure 19 - Wake Velocity and Pressure Profiles, $\alpha = 10.3°$

40

x = 110% c.

Figure 19 - Continued

41
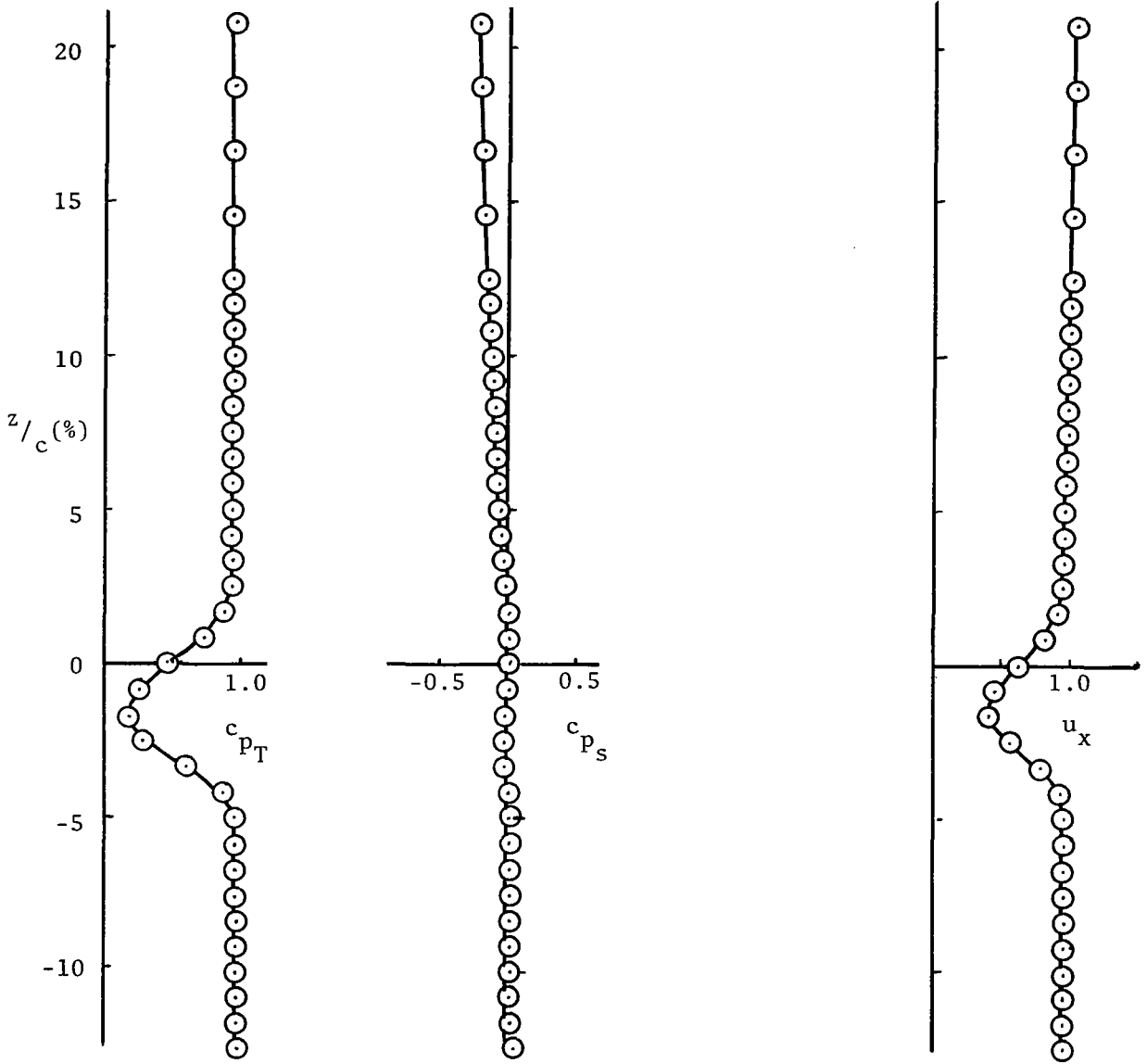
x = 120% c

Figure 19 - Continued

42
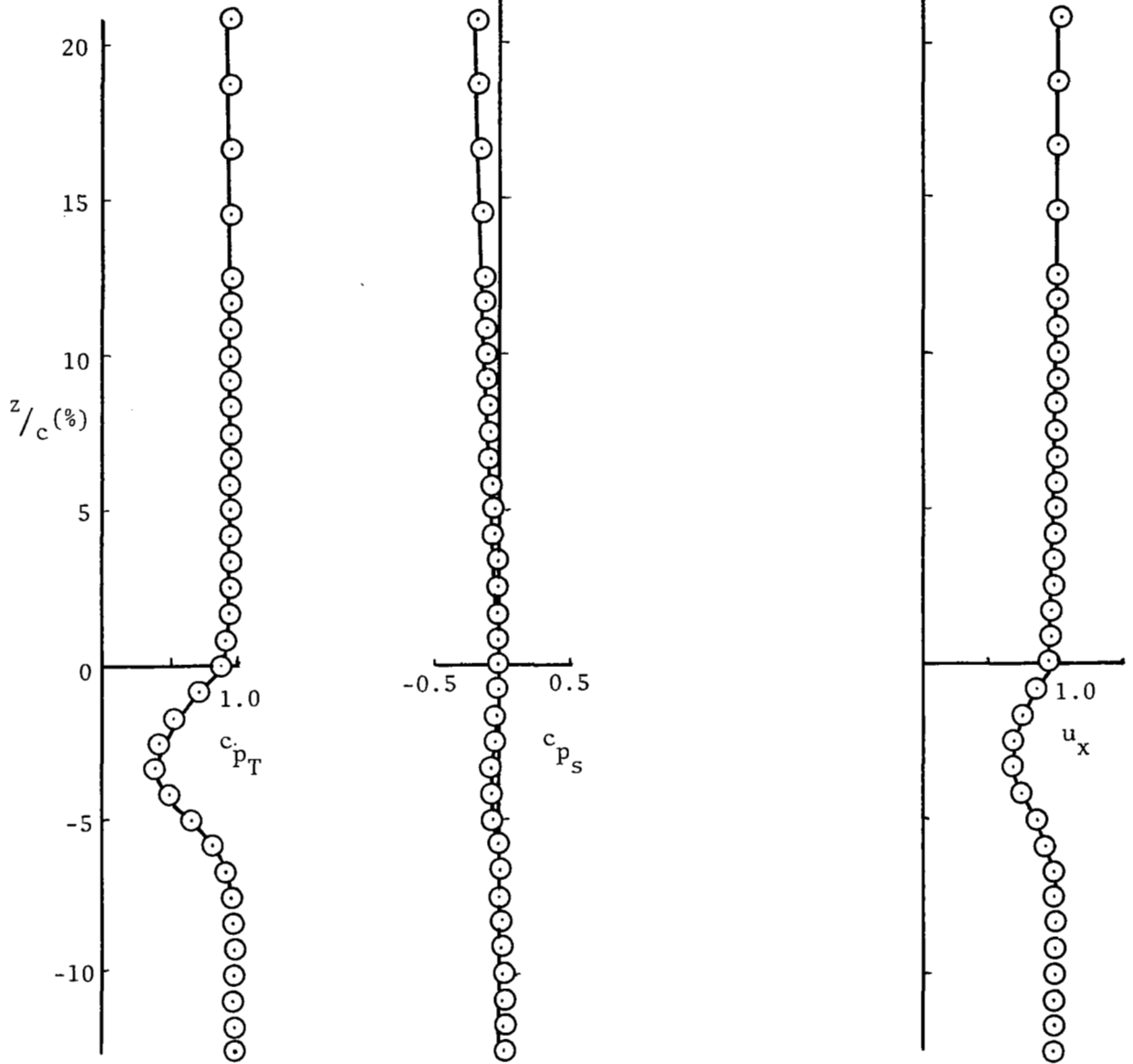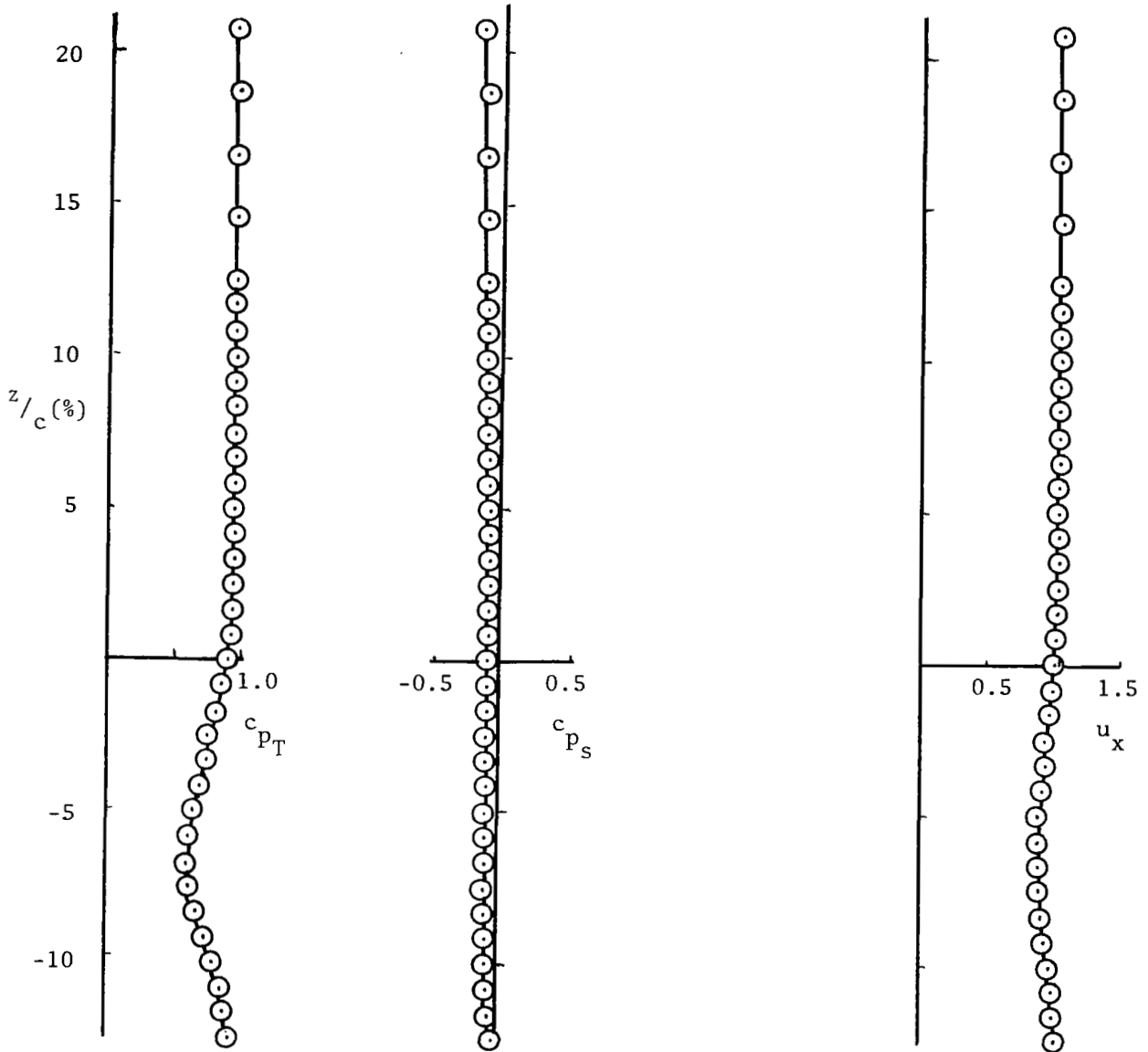
x = 150% c

Figure 19 - Concluded

X = 105.6% c
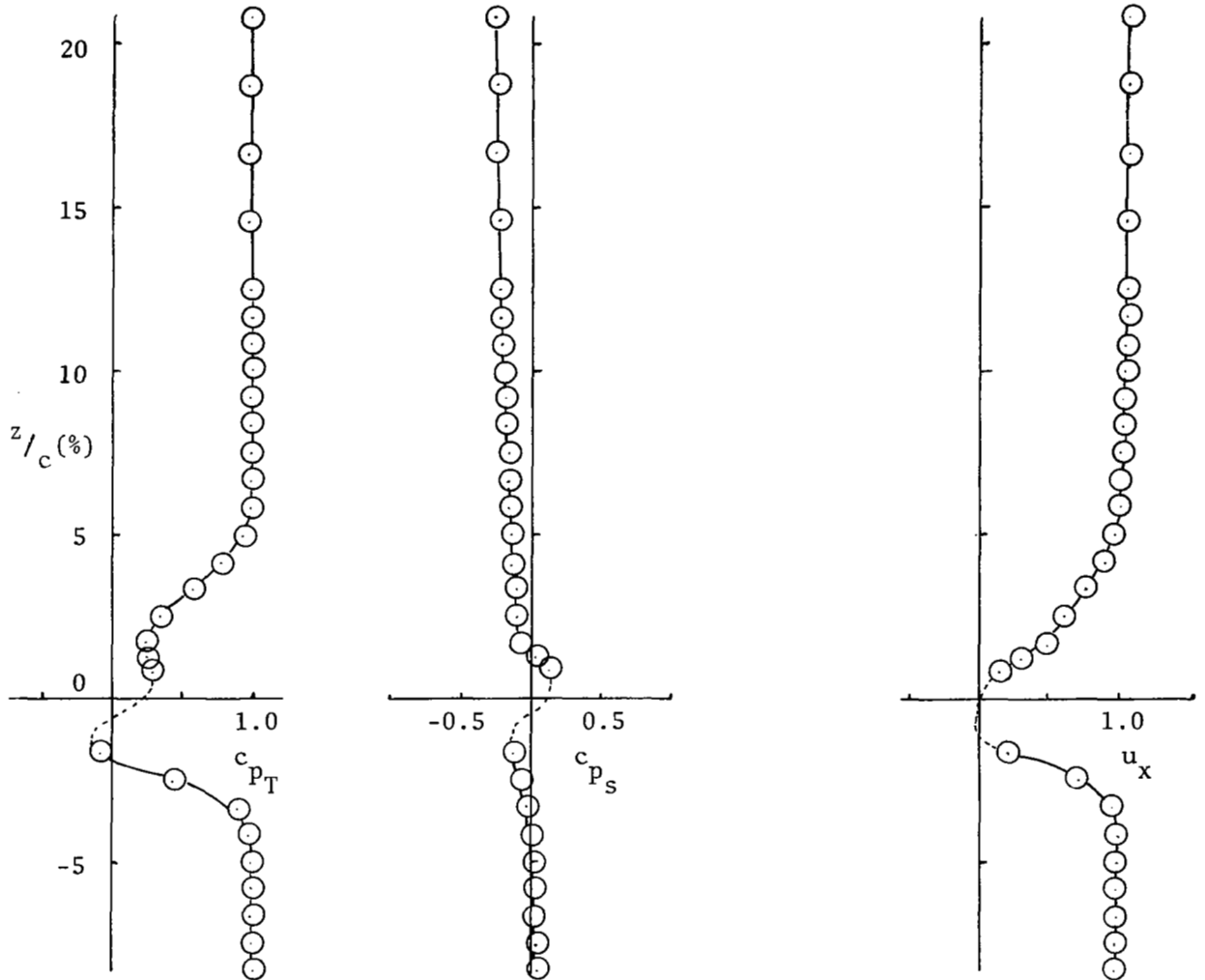
Figure 20 - Wake Velocity and Pressure Profiles, $\alpha = 14.4°$

44

x = 110% c

Figure 20 - Continued.

45
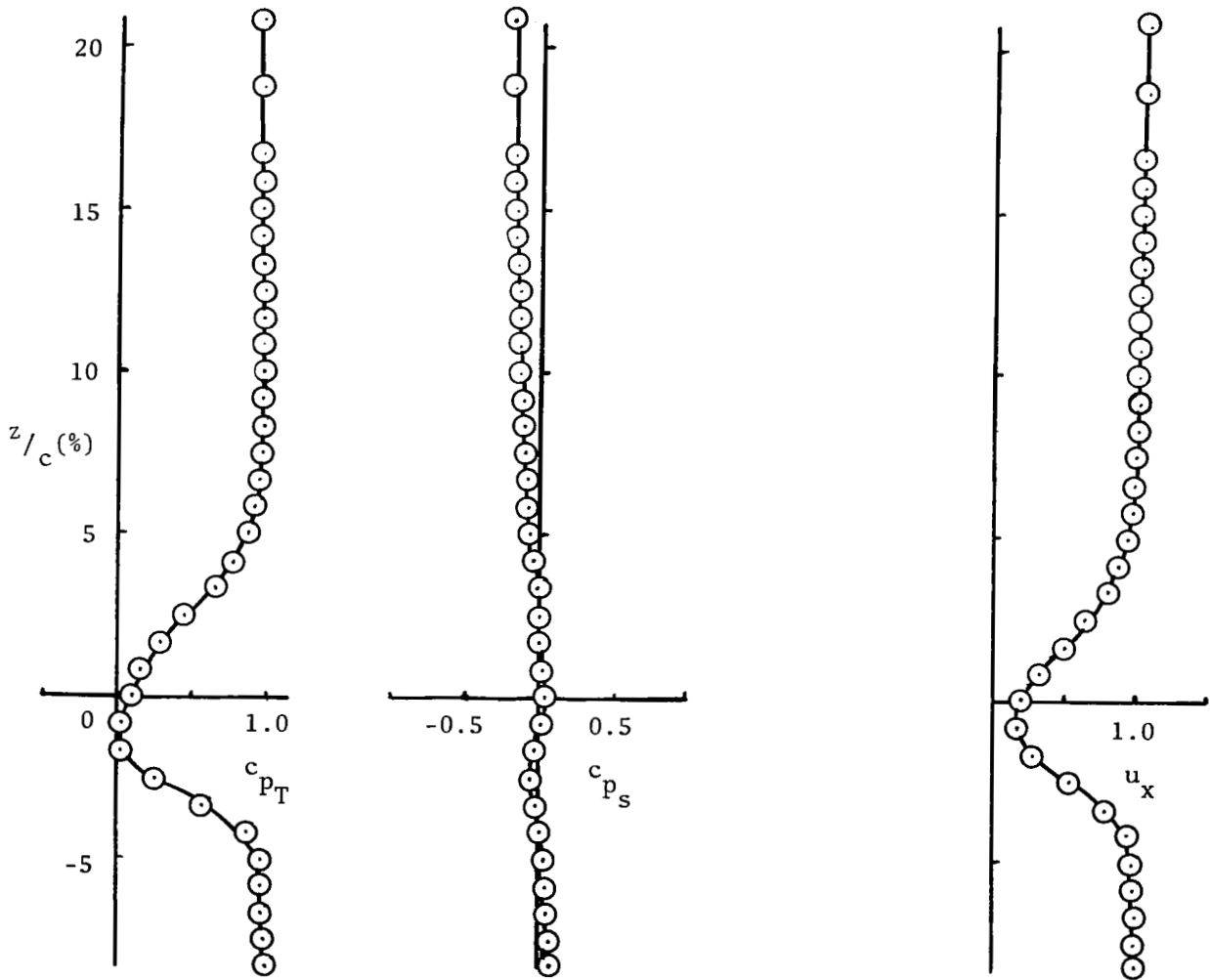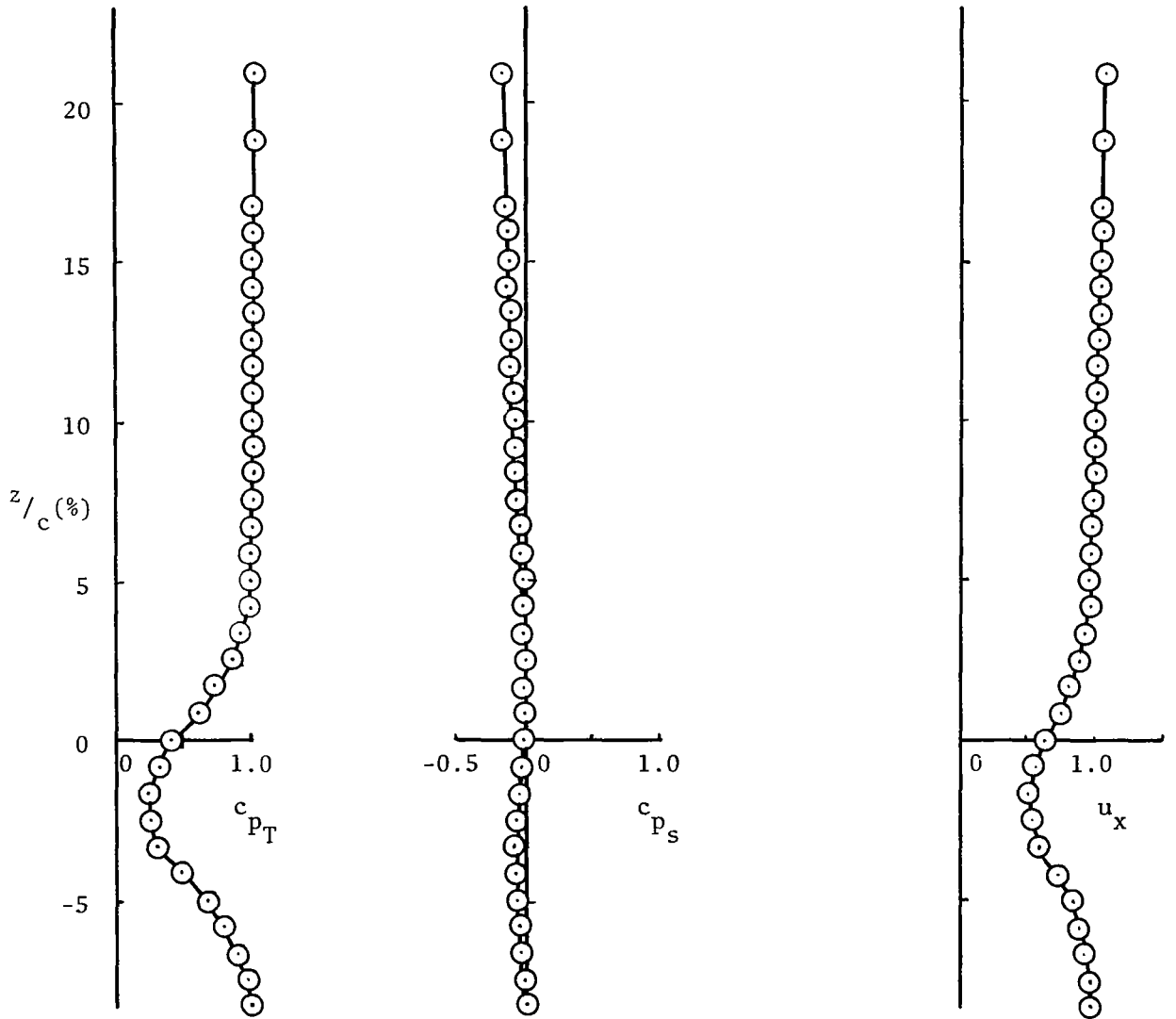
x = 120% c

Figure 20 - Continued.

x = 150% c

Figure 20 - Concluded.

x = 105.6% c

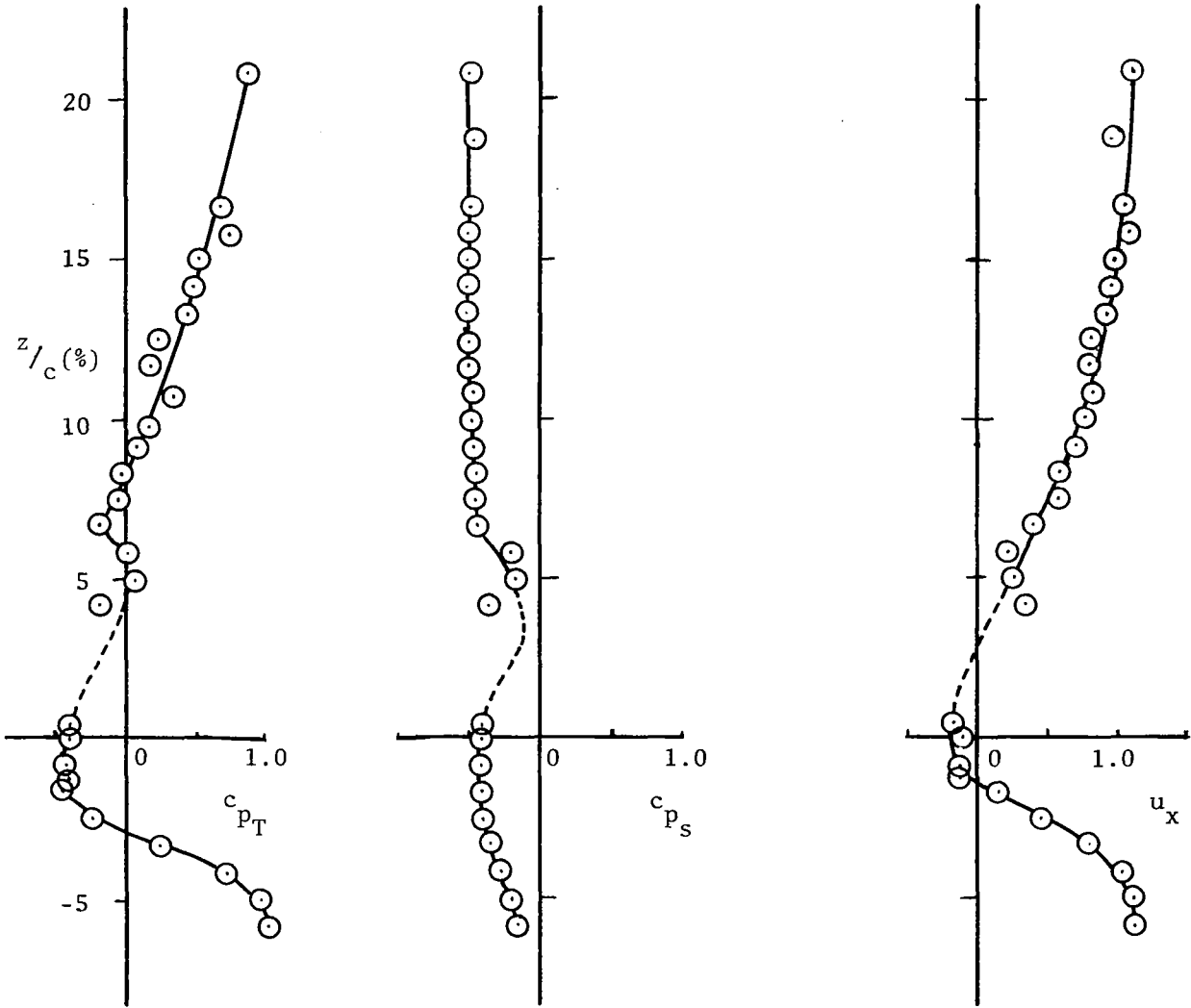Figure 21 - Wake Velocity and Pressure Profiles, α = 18.4°
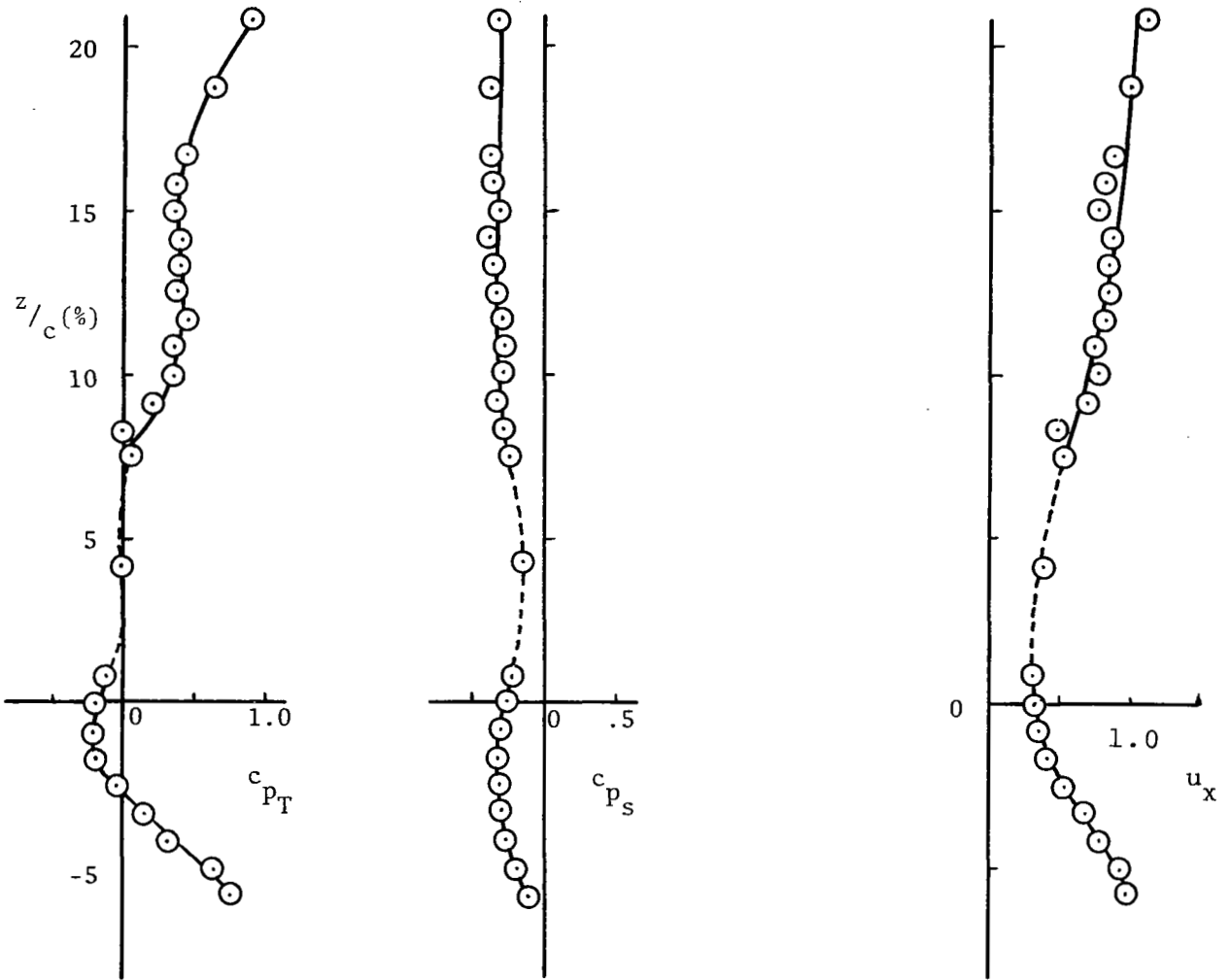
x = 110%c

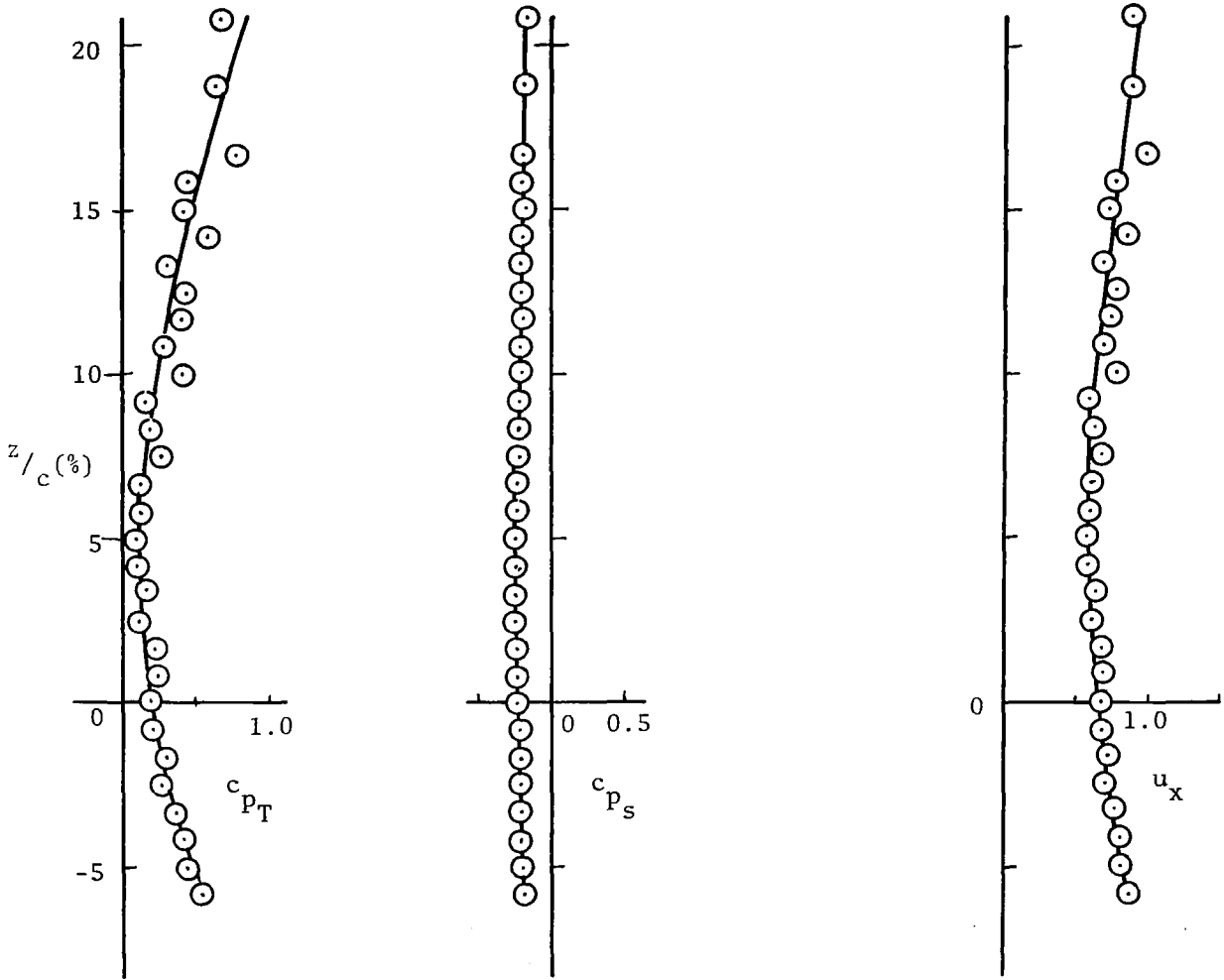Figure 21 - Continued.
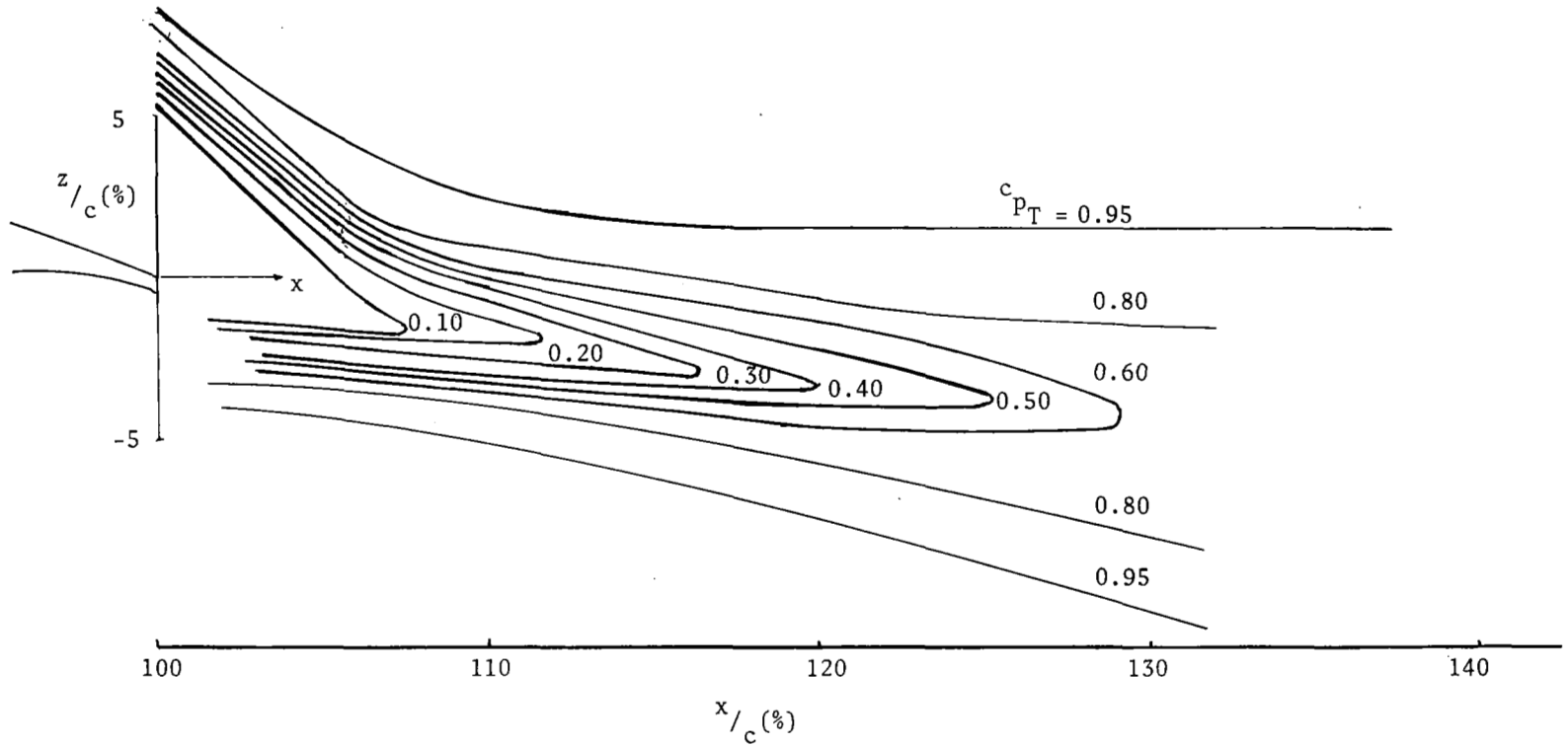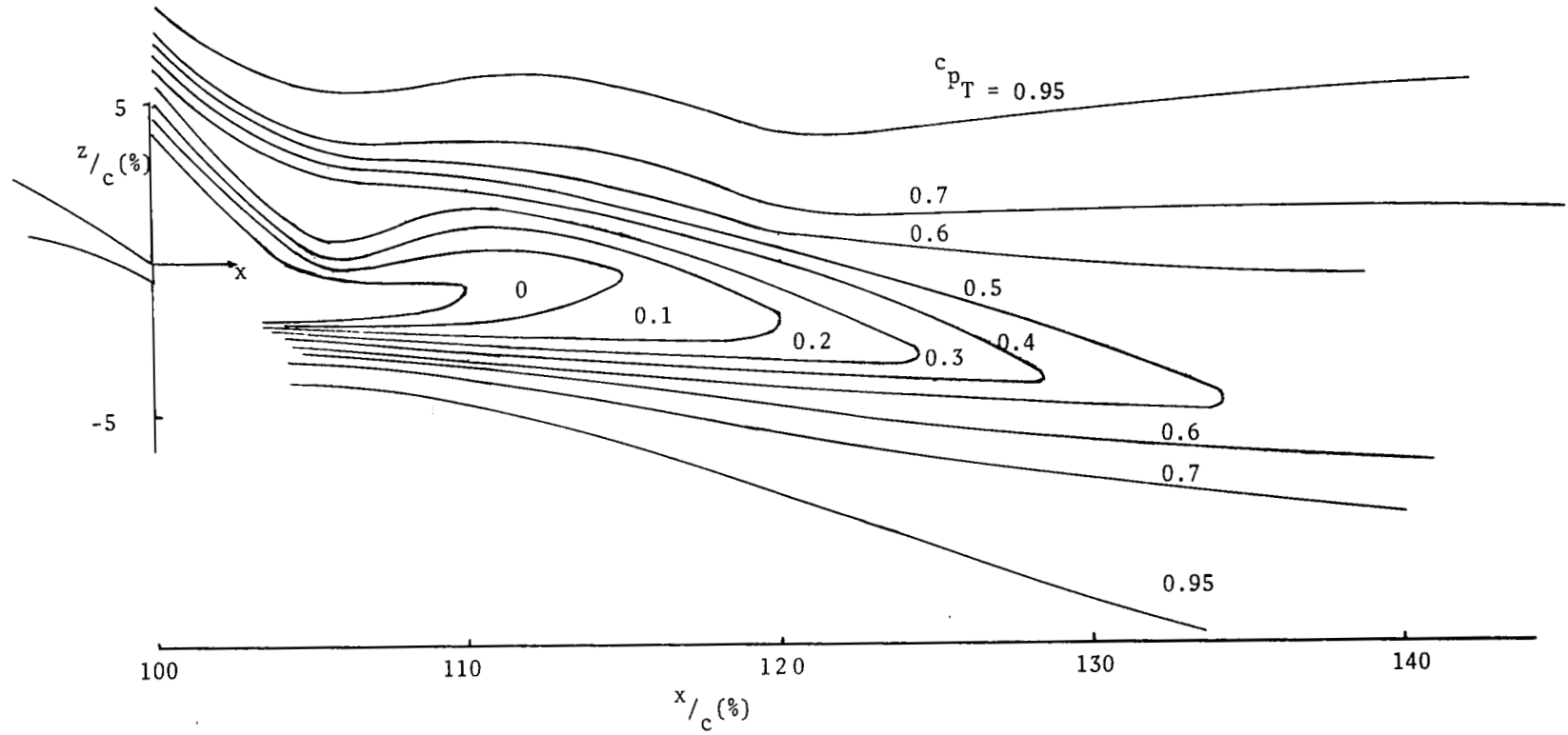
x = 120%c

Figure 21 - Continued.

x = 150%c

Figure 21 - Concluded.

Figure 22 - Wake Total Pressure Contours, $\alpha = 10.3°$

Figure 22 - Continued, $\alpha = 14.4°$

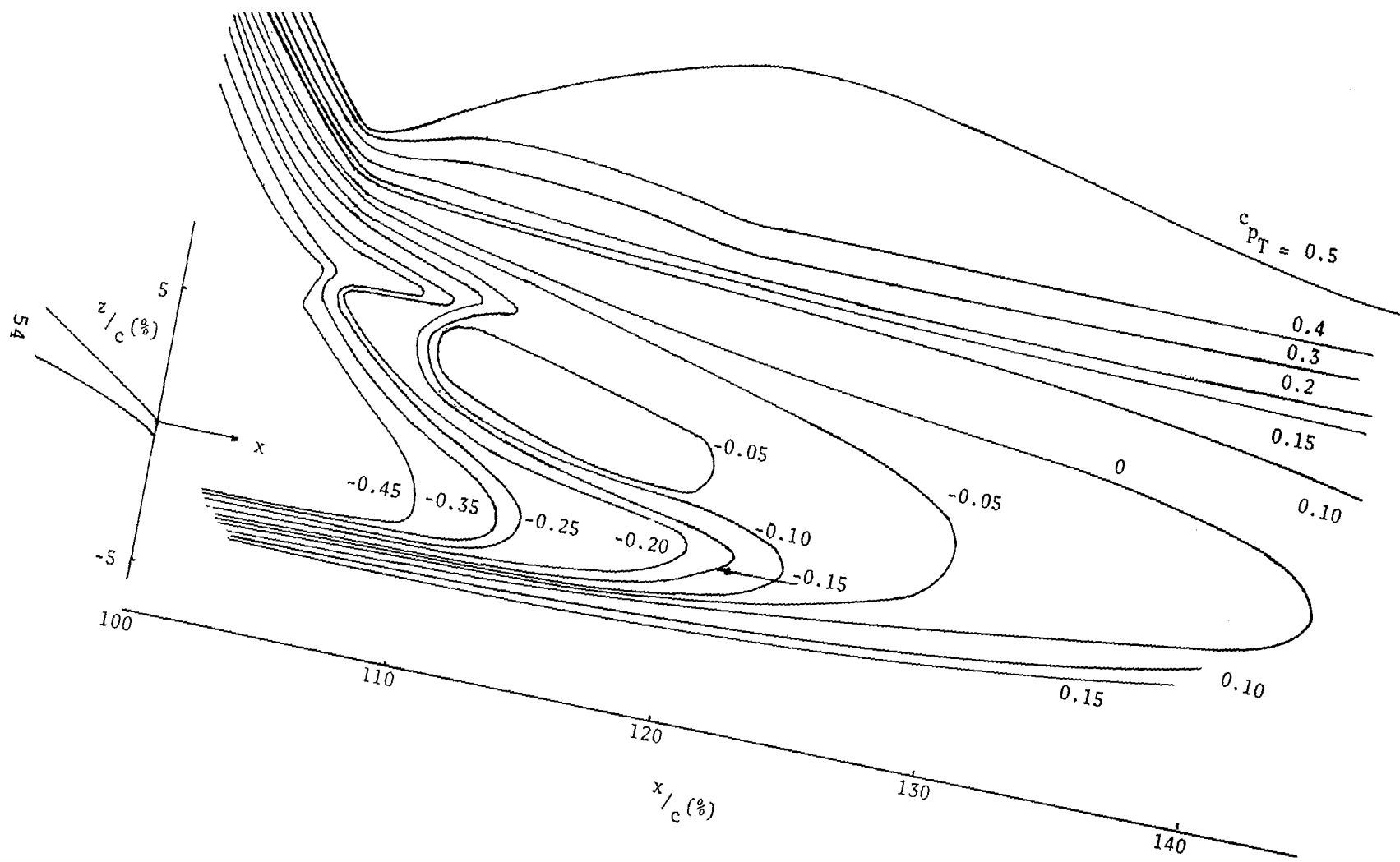Figure 22 - Concluded. $\alpha \approx 18.4°$

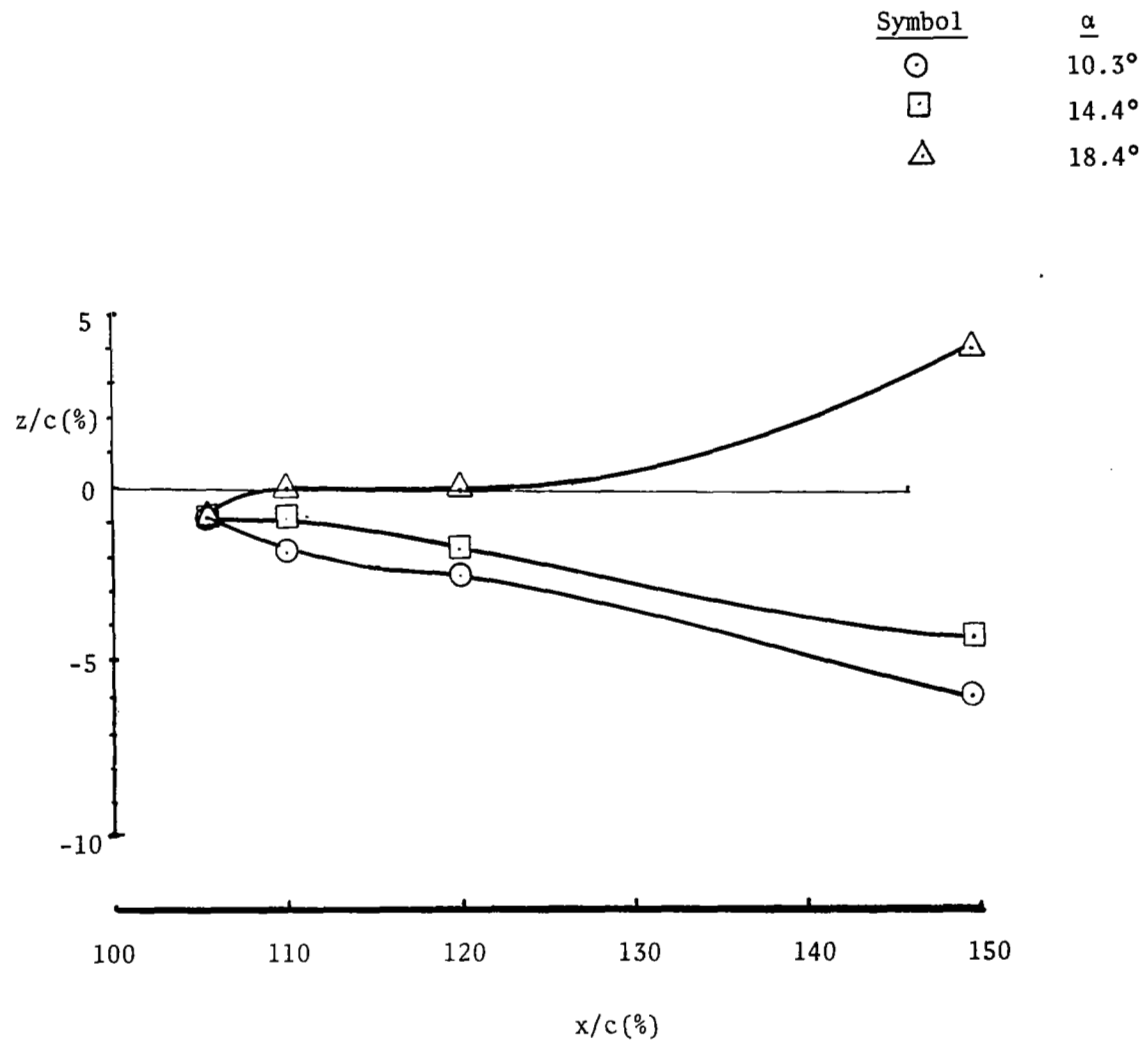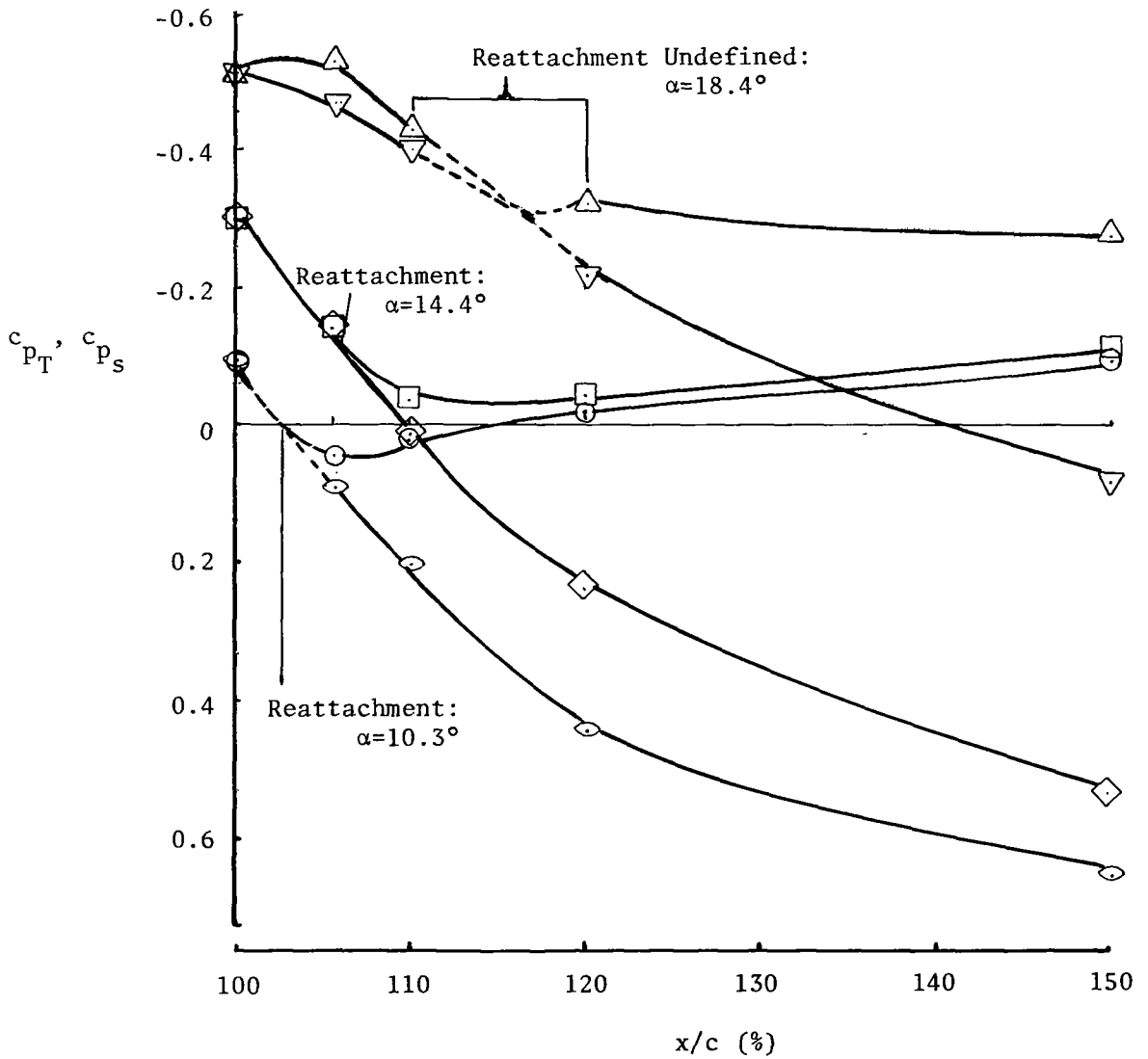| Symbol	α
⊙	10.3°
⊡	14.4°
△	18.4°

Figure 23 - Wake Center Locations

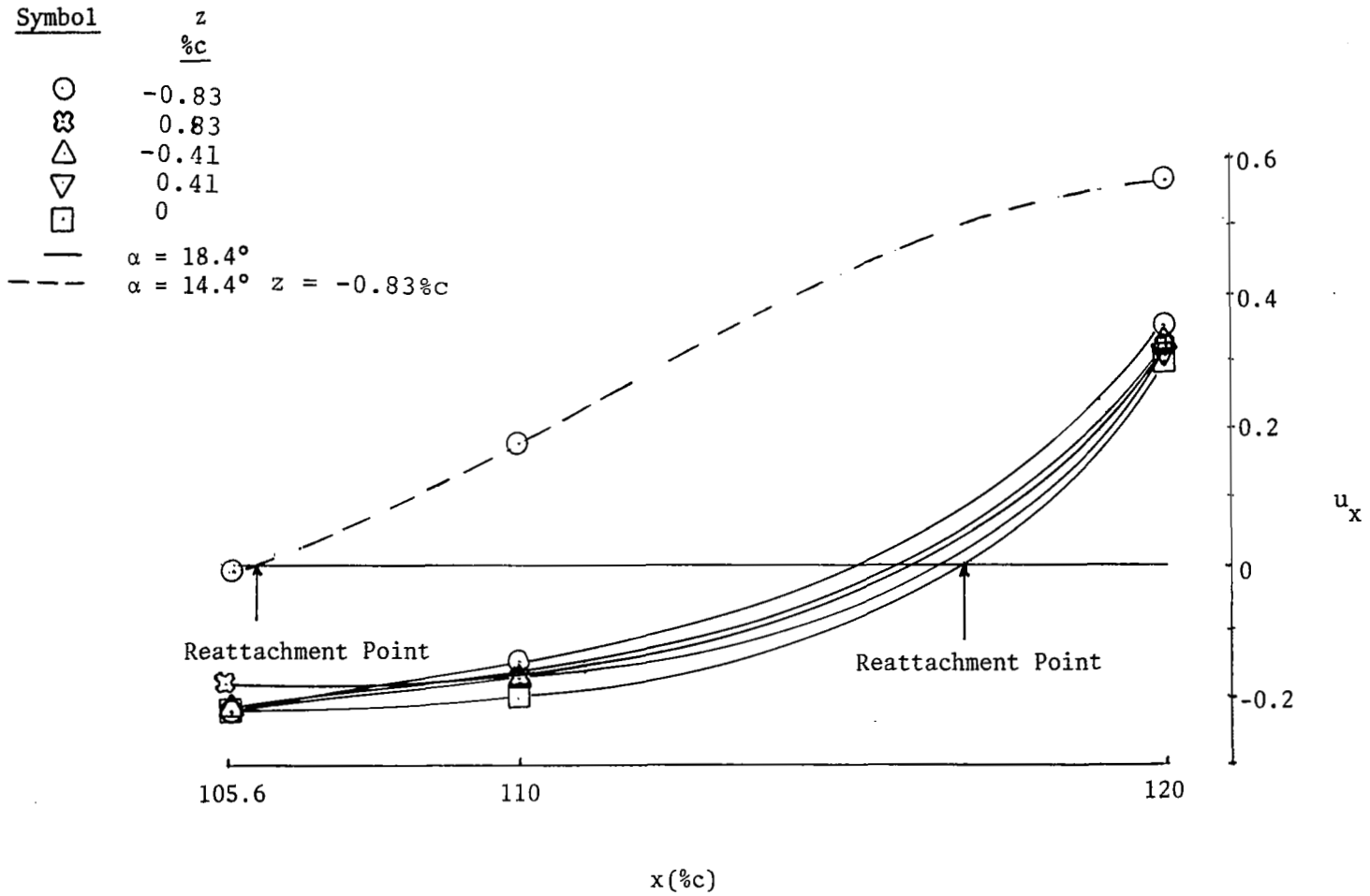Figure 24 - Total and Static Pressures Along Wake Centerlines

Figure 25 - Determination of Reattachment Point Locations

APPENDIX

Corrections to Velocity Probe Positions
for Model Aeroelastic Effects

Pitot probe positions were set with the probe initially
touching the surface of the airfoil, before the start of the
tunnel run. When the required speed is established in the
tunnel, aerodynamic loads cause the wing and balance system
to deflect relative to the probe. For upward deflections
of the wing, the flexible probe tip deflects such that con-
tact with the wing surface continues for two or three "nominal"
probe settings. This effect appears as a discontinuity in
slope of the indicated velocity profiles. Examples of this
are shown in Figure A1, which show constant or nearly constant
velocities very near the surface. This effect and the method
of correcting for it have been described in Reference 10, and
are illustrated by the figure. Corrections obtained in this
manner have been applied to velocity profiles forward of the
50% c location.

A second method for determining model deflections was to
carry out a static loading calibration, simulating test forces
and moments. This loading results in vertical translation,
horizontal translation, and balance rotation about the 50% c
point. Since the airfoil was restrained in torsion at only
one end, it is also necessary to account for elastic deflec-
tions due to wing spar torsion. An additional correction due
to mechanical backlash in the pitch mechanism has also been
included.

This calibration results in the deflections tabulated
in Tables A1, A2 and A3. Maximum upward deflection is about
0.15% c near the leading edge, and maximum downward deflec-
tion is 0.125% at the trailing edge. For positions forward
of mid-chord, the deflections obtained from static loading
agree within .025% c with those obtained from the method of
Reference 10. For positions aft of 50% c, the airfoil deflects

downward, opening the probe-airfoil gap. Corrections to these profiles have been made based upon the static loading data.

TABLE A1: Airfoil Deflections Under Load, $\alpha = 10.3°$

Lift = 890 Newtons (200 lbs)

Pitching Moment: 107 Newton-Meters (950 lb-ins)

Drag: 40 Newtons (9 lbs)

x, % c	Δz Drag % c	Δz Lift % c	Δz Pitching Moment % c	Δz Torsion % c	Δz Mechanical Backlash (α=.1° Max) % c	Δz Total % c
5	-0.0896	0.0250	0.0875	0.0092	0.0792	0.1113
10	-0.0540	0.0250	0.0775	0.0079	0.0708	0.1275
20	-0.0260	0.0250	0.0580	0.0063	0.0525	0.1167
30	-0.0140	0.0250	0.0388	0.0042	0.0350	0.0917
40	-0.0030	0.0250	0.0199	0.0021	0.0173	0.0608
50	0.0067	0.0250	0.	0.	0.	0.0317
70	0.0360	0.0250	-0.0388	-0.0042	-0.0350	-0.0163
80	0.0450	0.0250	-0.0583	-0.0063	-0.0525	-0.0475
90	0.0480	0.0250	-0.0775	-0.0079	-0.0708	-0.0829
100	0.0480	0.0250	-0.0958	-0.0104	-0.0875	-0.1192

TABLE A2: Airfoil Deflections Under Load, $\alpha = 14.4°$

Lift = 1068 Newtons (240 lbs)

Pitching Moment: 129 Newton-Meters (1140 lb-ins)

Drag: 58 Newtons (13 lbs)

x, % c	Δz Drag % c	Δz Lift % c	Δz Pitching Moment % c	Δz Torsion % c	Δz Mechanical Backlash (α=.1° Max) % c	Δz Total % c
5	-0.1125	0.0292	0.1067	0.0113	0.0792	0.1137
10	-0.0667	0.0292	0.0946	0.0104	0.0708	0.1383
20	-0.0325	0.0292	0.0708	0.0079	0.0525	0.1279
30	-0.0175	0.0292	0.0475	0.0050	0.0350	0.0992
40	-0.0041	0.0292	0.0238	0.0025	0.0173	0.0688
50	0.0083	0.0292	0.	-	-	0.0375
65	0.0367	0.0292	-0.0354	-0.0038	-0.0267	0.0004
75	0.0521	0.0292	-0.0592	-0.0063	-0.0433	-0.0283
90	0.0608	0.0292	-0.0946	-0.0113	-0.0708	-0.0833
100	0.0608	0.0292	-0.1183	-0.0125	-0.0875	-0.1292

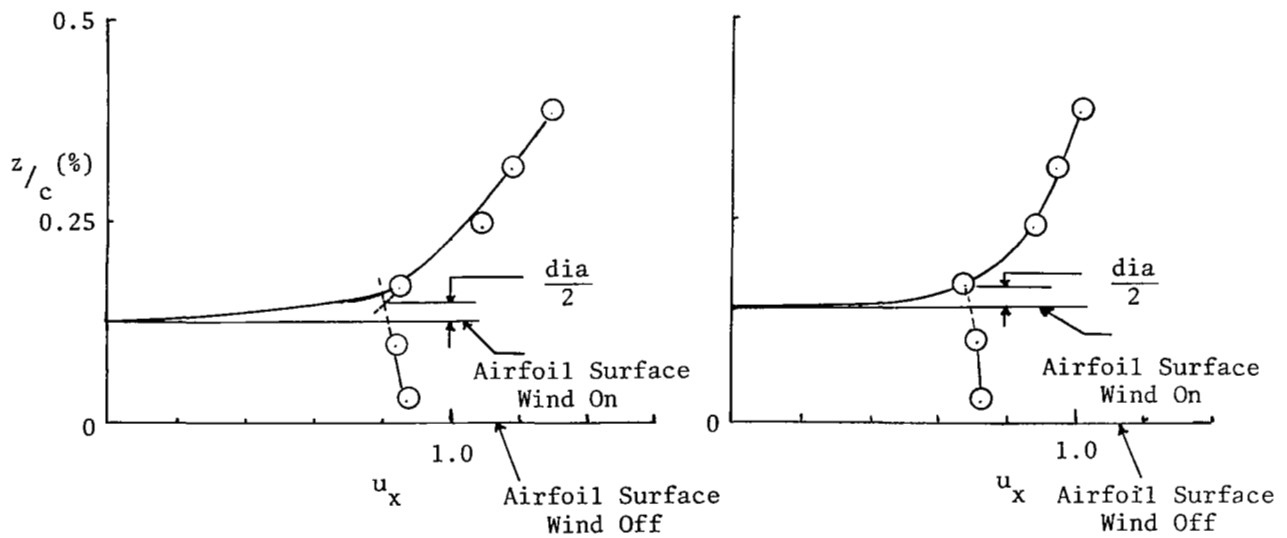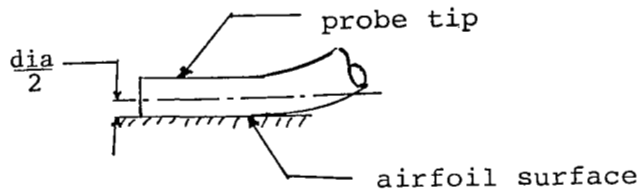TABLE A3: Airfoil Deflections Under Load, $\alpha = 18.4°$

Lift = 1068 Newtons (240 lbs)

Pitching Moment: 129 Newton-Meters (1140 lb-ins)

Drag: 111 Newtons (25 lbs)

x, % c	Δz Drag % c	Δz Lift % c	Δz Pitching Moment % c	Δz Torsion % c	Δz Mechanical Backlash (α=.1° Max) % c	Δz Total % c
5	-0.1375	0.0292	0.1067	0.0113	0.0792	0.1000
15	-0.0550	0.0292	0.0917	0.0092	0.0617	0.1363
25	-0.0396	0.0292	0.0654	0.0063	0.0433	0.1054
35	-0.0133	0.0292	0.0392	0.0038	0.0267	0.0833
45	0.0025	0.0292	0.0129	0.0013	0.0092	0.0546
60	0.0325	0.0292	-0.0263	-0.0025	-0.0175	0.0154
75	0.0638	0.0292	-0.0592	-0.0063	-0.0433	-0.0229
82.5	0.0696	0.0292	-0.0850	-0.0079	-0.0567	-0.0500
90	0.0742	0.0292	-0.0946	-0.0113	-0.0708	-0.0829
100	0.0746	0.0292	-0.1183	-0.0125	-0.0875	-0.1258

a) Near the leading edge.   b) Near mid-chord.

Figure A1 - Determination of airfoil deflection from velocity profile data.